Research review and prospects of the 2000 giant Yigong long-runout landslide: Volume, formation mechanism and recurrence period, Tibetan plateau, China

Changbao Guo[1,2]*, Hao Yuan[1]*, Ruian Wu[1,2], Yiqiu Yan[1] and Zhihua Yang[1,2]

[1]Institute of Geomechanics, Chinese Academy of Geological Sciences, Beijing, China, [2]Key Laboratory of Active Tectonics and Geological Safety, Ministry of Natural Resources, Beijing, China

The long-runout landslide is an unusual landslide with great drop height, long sliding distance, large volume, and high velocity, which is characterized by strong kinetic energy, fragmentation and entrainment effect. The landslide and its induced hazard chain may produce serious consequences. Based on remote sensing interpretation, field investigation and simulation, this paper summarizes the research progress of the 2000 giant Yigong long-runout landslide in Tibet, analyzes the initiating mechanism, volume and sliding velocity of the Yigong landslide, and further reveals that endogenic and exogenic geological processes are the main influencing factor of the Yigong landslide. It is also found that the landslide has a periodic initiating mechanism with characteristics of head-cut and recurrence. However, there are great differences in the existing studies on the volume of the slide source zone in the Yigong landslide. This paper calculates the landslide volume based on ArcGIS spatial analysis and obtains an initial landslide volume of approximately $9.225 \times 10^7 \, \text{m}^3$. The landslide final deposition volume is approximately $2.81 \sim 3.06 \times 10^8 \, \text{m}^3$, which is consistent with the other researchers. Moreover, there are two potential dangerous rock mass in the slide source zone, with a total volume of approximately $1.86 \times 10^8 \, \text{m}^3$. Dangerous rock mass may form the hazard chain of landslide-river blockage-dam break again and lead to significant disasters. Hence, we suggest the following research on Yigong landslide: Stability of the potential dangerous rock mass in the slide source zone, the prediction of the hazard chain, monitoring and early warning for the landslide. It is of great significance to guide the construction of major projects such as railway and hydropower projects and hazard prevention and mitigation in this area.

KEYWORDS

Yigong, long run-out landslide, slip mechanism, landslide volume, hazard chain

1 Introduction

The long-runout landslide refers to an unusual landslide with great drop height, long sliding distance, large volume, and high velocity. In detail, the elevation drop of the landslide is greater than hundreds of meters, the equivalent friction coefficient of H/L (H is the elevation drop and L is the horizontal sliding distance) is lower than 0.6, the landslide volume is greater than $10^6\ \text{m}^3$, and the velocity is generally greater than 20 m/s, mostly 40–80 m/s, and the maximum is bigger than 200 m/s (Hsu, K. J., 1975; Clague et al., 1987; Cheng et al., 2007; Zhang et al., 2010; Hungr et al., 2014; Yin et al., 2017; Zhang et al., 2022). The long-runout landslides are developed all over the world. They are characterized by strong kinetic energy, fragmentation and entrainment effect, which also often produced severe damage. For example, in 2017, the Xinmo giant landslide in Mao County, Sichuan Province had an initial volume of approximately $450 \times 10^4\ \text{m}^3$ and an accumulation volume of approximately $1,637\ \times\ 10^4\ \text{m}^3$. It dropped over an elevation difference of 1,200 m, travelled 2,800 m in horizontal distance and caused Xinmo village buried and more than 90 people missing (Fan et al., 2017; He et al., 2017; Xu et al., 2017; Yin et al., 2017). In 2019, the Shuicheng giant landslide had an initial volume of approximately $70\ \times\ 10^4\ \text{m}^3$ and the accumulation volume of $191 \times 10^4\ \text{m}^3$, with the elevation drop of 465 m and a horizontal distance of 1,250 m. The landslide also destroyed 21 houses and killed more than 50 people (Gao et al., 2020; Li et al., 2020; Zheng et al., 2020; Zhuang et al., 2020). In 1974, the Mayunmarca landslide lasted approximately 3 min and travelled approximately 8.25 km in Peru, with an accumulation volume of approximately $10 \times 10^8\ \text{m}^3$, an average velocity of 36 m/s and an elevation drop of approximately 1870 m. The landslide destroyed Mayunmarca village and killed more than 450 people (Kojan et al., 1978).

The Tibetan Plateau is one of the most complex geological regions in the world. There are many geological hazards developed here. The long run-out landslides are typical geological hazards in this area and have attracted the attention of scholars from all over the world. The Yigong landslide that occurred in 2000 is one of the most famous long run-out landslides. It lasted 6 min, travelled approximately 10 km, and had an elevation drop of approximately 3,330 m (Yin, 2000; Liu, 2002; Shang et al., 2003; Xu et al., 2012). A landslide dam formed after the Yigong landslide occurred, with a length of 2.5 km, a width of 2.5 km, an average thickness of 60 and the volume of approximately $3.0 \times 10^8\ \text{m}^3$. The flood produced by the dam broke that reached the lower reaches of India. However, the initiating mechanism, sliding velocity and volume of the Yigong landslide are still under dispute (Evans et al., 2011; Delaney et al., 2015; Guo et al., 2020). Here this paper based on literature review, field investigations and remote sensing to analyze and summarize research progress on the initiating mechanism, landslide volume,

velocity, and recurrence period of the Yigong long-runout landslide. It is useful for geohazard assessment of the Yigong landslide to carry out research on the stability of potential dangerous rock mass in the slide source zone, the prediction of the hazard chain, monitoring and early warning for the landslide.
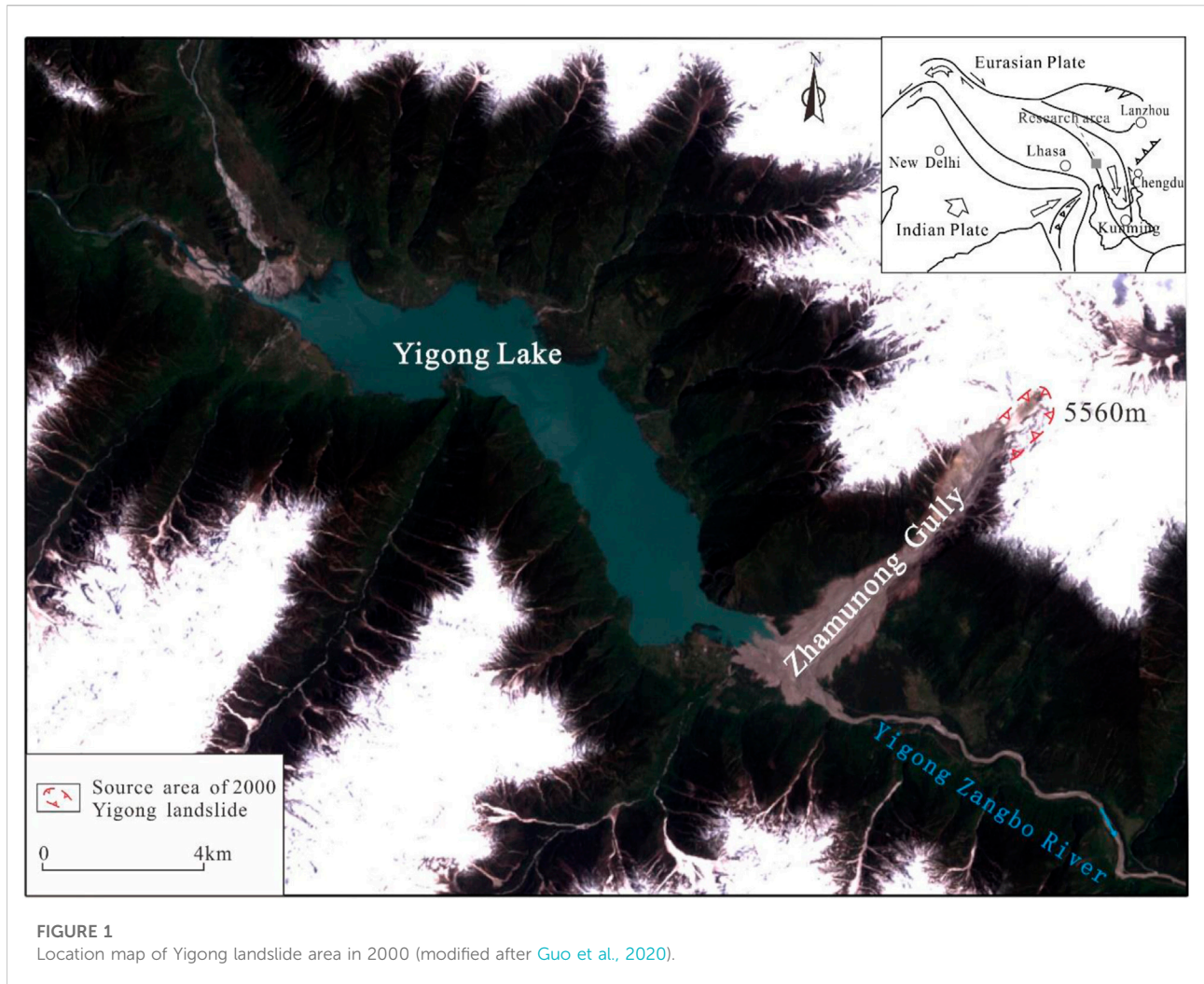
2 Geological background

2.1 Topography and geological structure

The Yigong landslide is located in the Zhamunong gully, Yigong Township, Bomi County, southeast Tibet. It is part of the middle and lower reaches of the Yigong Zangbo River. The average elevation in the area is more than 4,000 m. A V-shaped and deep-cut valley has developed, and the slopes of the canyon area are approximately 40°~60°. This area is a typical extremely high mountain canyon landform that also contains glacial landforms, such as ice buckets, horns, and moraine ridges. Precipitation in this area is concentrated in May to October, which accounts for approximately 78% of the annual precipitation. The annual average temperature is approximately 11.4°C. The temperature in winter is below zero, and there are large temperature differences between day and night and between seasons.

The Zhamunong gully is located at a position nearly orthogonal to the Yigong-Lulang fault and the Jiali fault. The tectonic movement is strong, and many earthquakes occurred in this area ago. The maximum earthquake magnitude in the area is the Chayu Ms8.6 earthquake in 1950. The slide source zone in the gully is an early Himalayan granite body. The bottom of the sliding source area is mainly composed of marble, sandstone, slate. Quaternary loose deposits are widely developed in the gully (Xu et al., 2012; Zhou et al., 2016).

2.2 Overview of the Yigong Landslide in 2000

On 9 April 2000, a long-runout landslide occurred in Yigong, Tibet. Yin (2020) believed that the initial landslide volume of approximately 100 million cubic meters at the rear edge of the Zhamunong gully collapsed from an altitude of approximately 5,520 m. The landslide lasted approximately 6 min, with an elevation drop of approximately 3,330 m. The collapsed rock mass quickly dropped and impacted the thick loose deposits in the trench. Then it formed a high-velocity rock avalanche with disintegration and entrainment. After travelling for approximately 10 km, the rock avalanche blocked the Yigong Zangbo River. The rock avalache formed a barrier dam with a length of approximately 2.5 km, an average thickness of 60 m, a thickness of up to 100 m at the thickest point (Figure 1). and a volume of approximately $3 \times 10^8\ \text{m}^3$ (Yin, 2000; Ren et al., 2001).

FIGURE 1
Location map of Yigong landslide area in 2000 (modified after Guo et al., 2020).

On 10 June 2000, the water from the Yigong barrier lake destroyed the open artificial diversion channel and rushed downstream. The water level at Tongmai Bridge 17 km away rose by 41.77 m, and the water level was approximately 32 m above the bridge deck. The flood washed away bridges, coastal roads, and communication facilities. Secondary hazards, such as collapses and landslides, were induced. Floods even spread downstream to India, causing hundreds of millions of economic losses downstream (Xu et al., 2012; Delaney et al., 2015; Xia, 2018).

3 Methods and data

3.1 Volume calculating methods based on remote sensing and GIS

The slide source zone of the Yigong long-runout landslide is located on a very high mountain with an altitude of approximately 5520 m, the drop elevation from the top of the landslide source to the Yigong Zangbo River is approximately 3330 m. Hence, the slide source zone of the landslide is out of sight of human beings. In addition, the landslide in 2000 occurred rapidly, and the landslide dam and the accumulation is in poor stability. As a result, conventional topographic surveying and mapping technology cannot reach the slide source zone for area and volume measurement. It is necessary to use appropriate technical methods to calculate the initial landslide volume and final deposition volume. With the development of aerial remote sensing and geographic information system technology, the high resolution and precision of remote sensing images obtained from the satellite have become higher. It has become possible to study the development and distribution characteristics of the large-scale long-runout landslide from the satellite and further provide data and support for the landslide investigation and mechanism research. Before and after the occurrence of the Yigong long-runout landslide in 2000, the Landsat 5, 7 and other satellites

launched by NASA (The National Aeronautics and Space Administration) obtained high-resolution remote sensing images of the landslide area. The SRTM (Shuttle Radar Topography Mission) task acquired a digital elevation model.

In this study, we collected the Landsat5 image acquired on 5 January 2000, the date before the Yigong landslide occurrence, the Landsat 7 image acquired on 4 May 2000, the date after the Yigong landslide occurrence, as well as the NASA DEM acquired from February 11 to 22 February 2000, the AW3D30 DEM acquired from January 2006 to May 2011. Based on ArcGIS spatial analysis technology, we calculated some parameters of the Yigong long run-out landslide, such as area and volume of formation and deposition zone.

3.2 Landslide running out analysis methods

The study of the Yigong-longrunout landslide sliding process is carried out by Massflow, a fluid and mechanics software. Massflow software is based on the MacCormack-TVD finite difference algorithm, which can efficiently simulate the dynamic evolution process of landslides, debris flows, and the movement process of long-runout landslides with large-scale, long-term migration, high-velocity, strong mobility (Ouyang et al., 2017; Ouyang et al., 2019; Yin et al., 2020; Li, 2021).

The Coulomb friction model is used in the slide source zone, where the bottom shear stress τ_b follows the Coulomb failure criterion (Eq. 1).

$$\tau_b = c + \rho g h \tan(\varphi) \tag{1}$$

where ρ is the density in kg $\bullet$ m^{-3}; h is the fluid height in m; c is the cohesion in kPa; and φ is the internal friction angle in °.

The movement simulation was used the Voellmy model, as in Eq. 2.

$$\tau_b = \mu \rho g h + \rho g \frac{V^2}{h \xi} \tag{2}$$

where μ is the friction coefficient, ξ is the turbulence coefficient, g is the acceleration of gravity in m/s^2 and V is the average velocity of the landslide mass in m/s. The scraping effect is represented by the erosion rate E of the base material, and the calculation formula of the erosion rate E is shown in Eq. 3.

$$E = \alpha h \sqrt{u^2 + v^2} \tag{3}$$

where h is the thickness of the sliding body in m, u is the moving velocity of the sliding body in the x direction in m/s, v is the moving velocity of the sliding body in the y direction in m/s, α is the average growth rate of erosion along the channel, and the calculation formula is shown in Eq. 4.

$$\alpha = \frac{\ln \left(V_f + V_0 \right)}{S} \tag{4}$$

where V_f is the final volume of the landslide in m^3, V_0 is the initial volume of the landslide in m^3, and S is the average erosion distance in m.

By inputting the inversion parameters in the simulating model, such as the effective friction coefficient, pore water pressure coefficient and cohesion force, the parameters of Yigong long-runout landslide's sliding velocity, accumulation thickness evolution process, furthest sliding distance, maximum accumulation thickness and accumulation range are calculated and figured out, and then the whole process of Yigong long-runout landslide movement is analyzed by stages.

3.3 Simulation parameters

The selection of parameters were obtained by trial-and-error inversion. The reference standards for the inversion results include the moving distance, velocity, entrainment amount, entrainment position, and deposition zone characteristics of the Yigong landslide in 2000. At the same time, the simulation also refers to published results (Liu et al., 2017; Dai et al., 2019; Zhuang et al., 2020). The slide source zone set the Coulomb model, the fast movement and entrainment zone and the deposition zone set the Voellmy model. The parameters are also adjusted according to the characteristics of different zones (Table 1). Finally, the simulation results were in good agreement with the Yigong landslide in 2000.

4 Engineering geological characteristics of the Yigong landslide

4.1 Characteristics of spatial distribution

Yin et al. (2000) divided the Yigong landslide into four zones based on field investigation, the slide and collapse zone, rock debris zone, mixed flow and wave zone and throwing accumulation zone. Huang (2004) and Xu et al. (2007) divided the landslide into three zones, including the collapse zone, sliding zone and deposition zone, according to the characteristics of material movement and accumulation in different parts during the hazard. In addition, the sliding zone is subdivided into the instantaneous high-velocity sliding zone and high-velocity rock-debris flow circulation zone. The deposition zone is subdivided into the block rock deposition zone, debris, the sand and dust deposition zone, the entrainment-debris deposition zone, and the air wave influence zone. Dai et al. (2019) and Zhuang et al. (2020) divided the landslide into the source area, entrainment area and deposit area, according to remote sensing images of before and after the landslide and field investigation. Liu et al. (2020) divided the landslide into the

TABLE 1 Model and simulation parameters.

Model	Parameters	The slide source zone (H ≥ 4,150)	The fast movement and entrainment zone (2,700 < h ≤ 4,150)	The deposition zone-I (2,400 < H ≤ 2,700)	The deposition zone -II (H ≤ 2,400)
Coulomb	$tan(\varphi)$	0.36	—	—	—
	c (Kpa)	10	—	—	—
Voellmy	μ	—	0.02	0.03	0.08
	ξ	—	1800	1,600	900
Entrainment	α	—	1.194×10^{-4}	—	—

H—Elevation in DEM model.
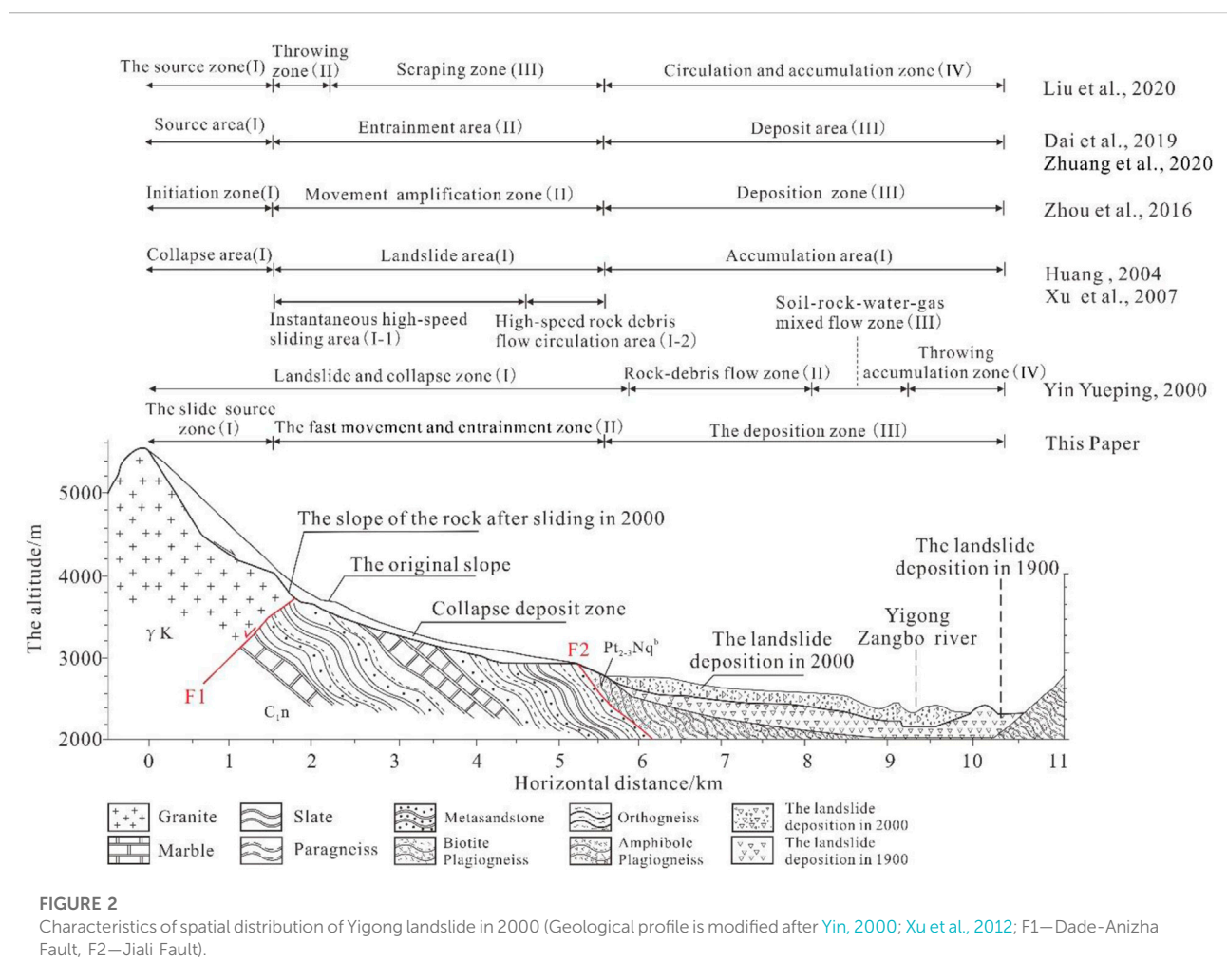
FIGURE 2
Characteristics of spatial distribution of Yigong landslide in 2000 (Geological profile is modified after Yin, 2000; Xu et al., 2012; F1—Dade-Anizha Fault, F2—Jiali Fault).

source zone, throwing zone, entrainment zone and circulation and deposition zone.

This paper suggests dividing the landslide into three zones (Figure 2), the slide source zone (I), the fast movement and entrainment zone (II) and the deposition zone (III).

4.1.1 The slide source zone (I)

The Yigong landslide source zone is located in the trailing part of Zhamunong gully, with an altitude range of approximately 4,400–5,300 m and a projected horizontal length of 1,390 m. The zone is covered with ice and snow all

FIGURE 3
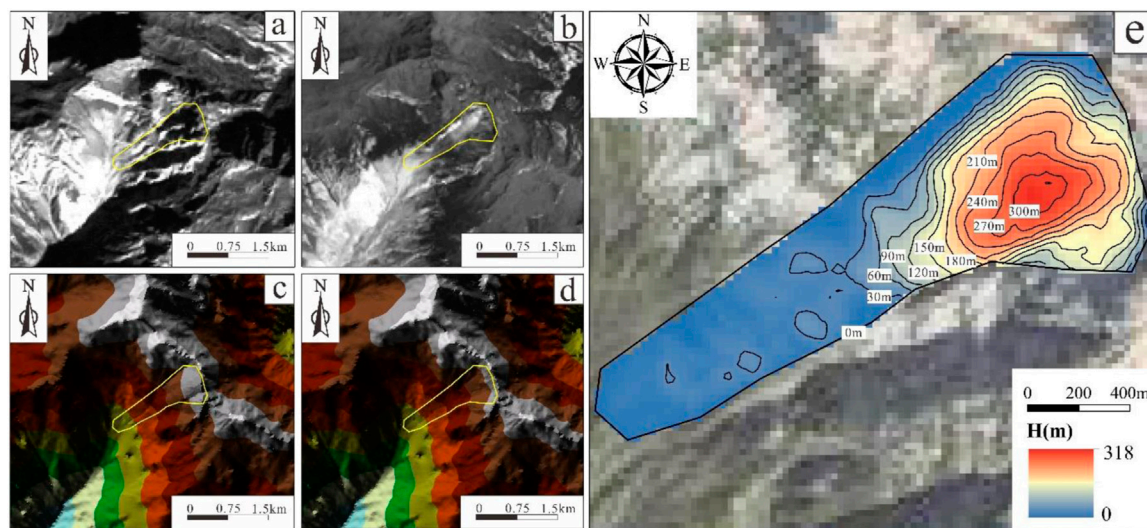Comparison of Yigong Landslide's slide source zone before and after sliding in 2000 **(A,B)**-the images are Landsat5 and 7 images, according to USGS: http://glovis.usgs.gov/; **(C,D)**-the tin files generated after terrain restoration based on AW3D30 DEM, according to JAXA (Japan Aerospace Exploration Agency), https://www.eorc.jaxa.jp/ALOS/en/aw3d30; **(E)**-restored sliding body of 2000 Yigong Landslide).

year. Affected by earthquakes, structure, and climate change, the dry-wet cycle and freeze-thaw weathering are strong in this zone. Joints and cracks are developed in the exposed bedrock, and the rock mass structure is broken. The rock mass of the source zone is controlled by three groups of joints, and their occurrences are $203\angle34°$, $94\angle57°$ and $211\angle86°$. The joints with small dip angles control the formation of the sliding surface, and the joints with large dip angles promote the formation of trailing edge tensile cracks (Li et al., 2018). The landslide body is wedge-shaped, the lower part is narrow, and the upper part is wide. The elevation drop ranged from 0 to 318m, with an average thickness of 98.8 m and a volume of approximately $9,225 \times 10^4\,m^3$ (Figure 3). The deep V-shaped grooves left after the collapse are still visible. Affected by the rock mass structure, intense small and moderate earthquakes and climate change, the tailing edge of the slope will collapse again in the future.

4.1.2 The fast movement and entrainment zone (II)

The zone (II) is located in the upper part of Zhamunong gully, with an altitude range of approximately 2,900–4,400 m and slopes of approximately 16°~27°. This zone has a long and narrow shape, with collapse deposits on both sides and Quaternary loose deposits. After the landslide, the bedrock on both sides was exposed, and scratches are present, which indicates that there is strong entrainment effect. The simulation also shows that the landslide velocity in this area reaches the maximum, the maximum velocity is 95 m/s (Figure 4). The maximum of the entrainment depth is approximately 130 m in the middle and

upper part of the Zhamunong gully (Figure 5). The high-place gravitational potential energy obtained by the sliding body in this area is rapidly transformed into strong kinetic energy. The sliding body disintegrated due to the velocity difference and collision effect. Finally, the collapse turned into rock avalanche.

4.1.3 The deposition zone (III)

The deposition zone (III) is located in the middle and lower parts of Zhamunong gully, connected with the Yigong Zangbo River, with an altitude range of approximately 2,200–2,900 m and average slopes of approximately 5°–7°. Due to the terrain changes from narrow and steep to gentle and open, the rock avalanche decelerated and deposited here to form deposition fan. The rock avalanche also blocked the river to form a dam with an average thickness of 60 m and a maximum thickness of approximately 108 m. The dam was approximately 3227 m long, 1120 m wide and 3.34 km² area in this zone (Figure 5). In addition, there was a landslide in 1900, so the deposition of the 2000 landslide overlaid the deposition of the 1900.

4.2 Landslide volume

4.2.1 The initial landslide volume

Many scholars had studied the initial landslide volume. Yin (2000) believed that hundreds of millions of square meters of sliding body were saturated and unstable. Xue et al. (2000) deemed that approximately $1\times10^7\,m^3$ rock mass collapsed from the source zone. Liu (2002) revealed that before the

FIGURE 4
Velocity characteristics of different monitoring points.
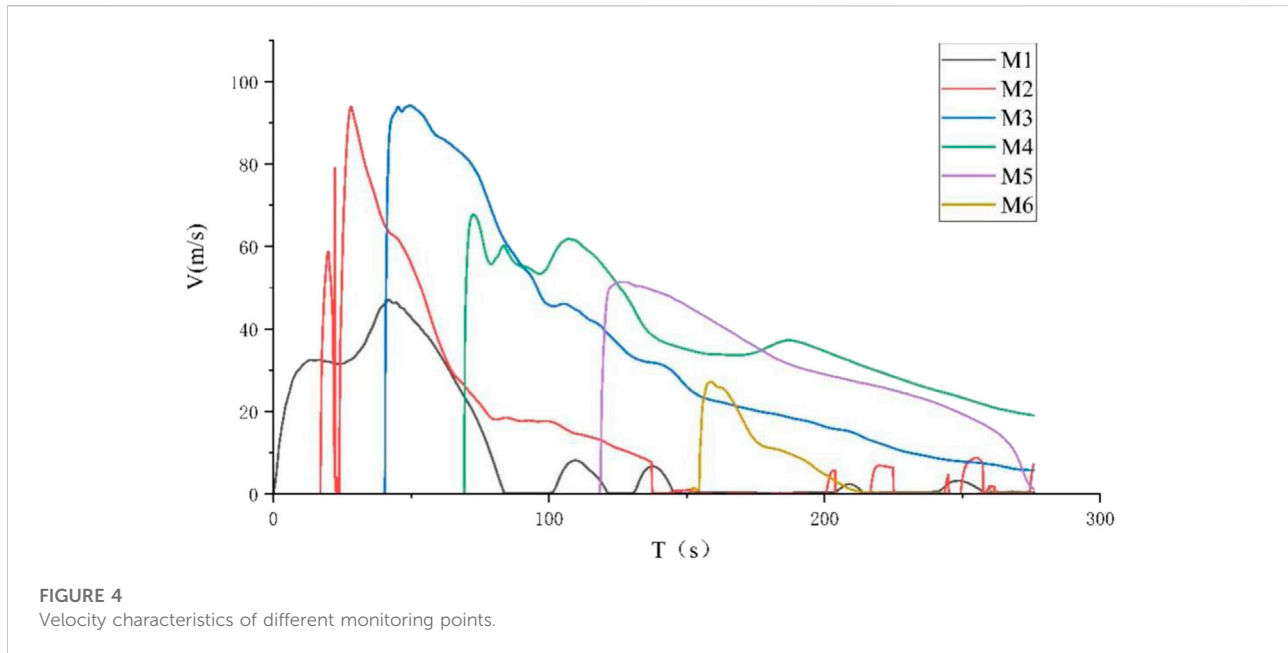
collapse, the landslide source zone was angular and peak-like, the rock mass slopes reached 50°~70°, and the exposed V-shaped grooves formed after the landslide. He estimated that initial landslide volume was approximately $3 \times 10^7 \, m^3$. Shang et al. (2003), Yin et al. (2012), Zhou et al. (2016) and Zhuang et al. (2020) considered that the wedge-shaped saturated rock mass of approximately $1 \times 10^8 \, m^3$ in the source zone was unstable. Wang (2006) combined the comparative analysis of remote sensing images before and after the landslide on 9 April 2000, to determine the position of the block before sliding and the irregular polygonal structure with the upper width and lower width and the projected area of the sliding zone is approximately $0.691 \, km^2$. DEM analysis and image comparison show that the elevation drop of the slide source zone is between 0 and 318 m, and the initial landslide volume is $9.118 \times 10^7 \, m^3$. Evans et al. (2011) considered the volume of $9.118 \times 10^7 \, m^3$ to be unreasonable. He believed that the initial landslide volume is approximately $7.5 \times 10^7 \, m^3$, and the volume after fragmentation expansion is approximately $9 \times 10^7 \, m^3$. Xu et al. (2012) found that the initial landslide volume is $9 \times 10^7 \, m^3$. Delaney et al. (2015), through digital elevation model (DEM) data analysis and Landsat-7 image comparison, believed that the initial landslide volume of $9.1 \times 10^7 \, m^3$ was more credible, and the volume of the landslide after fragmentation expansion was approximately 1.2 times the initial volume (Table 2; Figure 6).

The Landsat images on January 5 and 4 May 2000, help to delineate the location of the slide source zone and indicate projected area of the source zone is approximately $7 \times 10^5 \, m^2$ (Figures 3A,B). The DEM data before the 2000 Yigong landslide was missing in the source zone, and the existing data were filled in the post-landslide DEM interpolation. Therefore, the topographic data before and after the slip in the source zone was recovered (Figures 3C,D) based on the field investigations and remote sensing interpretation. In this paper, AW3D30 is used as the original data for terrain restoration. Finally, the topographic differences before and the after the landslide show that the elevation of the sliding source zone decreases from 0 to 318 m (Figure 3E), the average thickness is 98.8 m, and the initial volume is approximately $9,225 \times 10^4 \, m^3$.

4.2.2 The final deposition volume

The landslide deposition body passed through and dammed the Yigong Zangbo River, forming a deposition zone with an altitude range of approximately 2,200–2,900 m and an area of approximately $5 \, km^2$. Yin (2000), Liu (2000), Zhou et al. (2000), Liu et al. (2001) and Huang et al. (2004) concluded that the deposition volume of the Yigong landslide was approximately $2.8~3.0 \times 10^8 \, m^3$. Zhou et al. (2016), Chai et al. (2001), Wang et al. (2002), Shang et al. (2003), Xu et al. (2012) and Zhuang et al. (2020) estimated that the deposition volume is approximately $3 \times 10^8 \, m^3$. Ren et al. (2001) found that the deposition volume exceeded $3.8 \times 10^8 \, m^3$, based on a comparison of portable global positioning system (GPS) field measurement data and remote sensing images before and after the landslide. After DEM analysis, Evans et al. (2011) shown that the entrainment volume of the Yigong landslide is $1.5 \times 10^7 \, m^3$, and the deposition volume was $1.05 \times 10^8 \, m^3$. Wang (2008) compared the slide source zone, the migration zone and the deposition zone and concluded that the deposition volume of $3 \times 10^8 \, m^3$ is unreasonable because the muddy water and strong air-sputtering area were not separated. It was considered more reasonable that the deposition volume was $9.11 \times 10^7 \, m^3$. The SRTM-3 DEM data and the Landsat-7
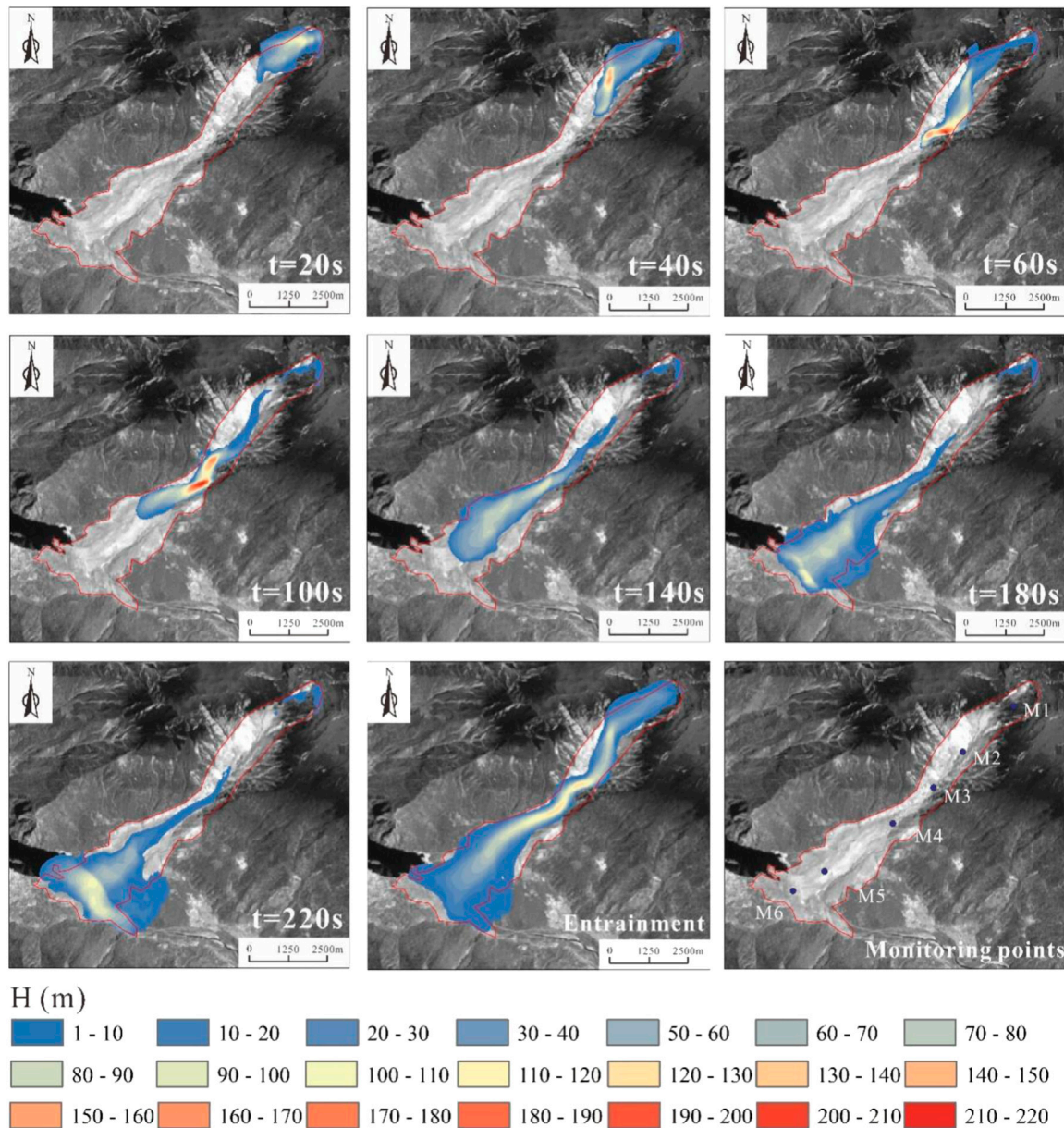
FIGURE 5
Simulation of motion process of the Yigong landslide in 2000 (The DEM used for the simulation is derived from NASA; https://earthdata.nasa.gov/).

images were used to calculate the final deposition volume of the Yigong landslide, which is 1.15×10^8 m³ (Delaney et al., 2015). Ekström et al. (2013) believed that the total mass of the Yigong landslide was 4.4×10^{11} kg. Assume that the average density of the rock mass is 2,630 kg/m³, the final deposition volume was able to calculate as approximately 1.67×10^8 m³. Liu et al. (2018) used digital terrain data from 1971 to 2003 to reconstruct the base sliding surface and calculated that the final deposition volume is approximately 1.29×10^8 m³ (Table 3; Figure 7).

Yin (2000) believed that the thickness of the deposits was 60 m on average, and the thickest part could reach 100 m, with an area of 5 km². Zhou et al. (2016) showed that the thicknesses of the tail part of the sedimentary area were approximately 4–10 m, the thicknesses of the middle part were approximately 35–65 m, and the thicknesses of the front part were approximately 50–80 m. Based on the remote sensing interpretation, this paper calculated that the landslide deposition zone has an area of approximately 5.1 km².

TABLE 2 Historical studies summary of the initial landslide volume of the Yigong landslide in 2000.

Number	Volume/m^3	Research methods	References
1	$>1 \times 10^8$	Field investigations, Estimate	Yin (2000)
2	1×10^7	Field investigations, Estimate	Xue et al. (2000)
3	3×10^7	Field investigations, Estimate	Liu (2002), Huang (200)4
4	4×10^7	Remote sensing interpretation	Zhang et al. (2013)
5	7.5×10^7	DEM data analysis, Remote sensing interpretation, Sliding body contour reconstruction	Evans et al. (2011)
6	9×10^7	DEM data analysis, Remote sensing interpretation, the entrainment effect	Delaney et al. (2015)
7	9.118×10^7	DEM data analysis, Remote sensing interpretation	Wang (2006)
8	1×10^8	Field investigation, Estimate	Shang et al. (2003), Yin et al. (2012), Zhou et al. (2016), Zhuang et al. (2020)
9	9.225×10^7	DEM data analysis, Remote sensing interpretation, Contour correction	This paper

DEM, digital elevation model; RS, remote sensing.

FIGURE 6
Summary of the initial landslide volume of the Yigong landslide in 2000.
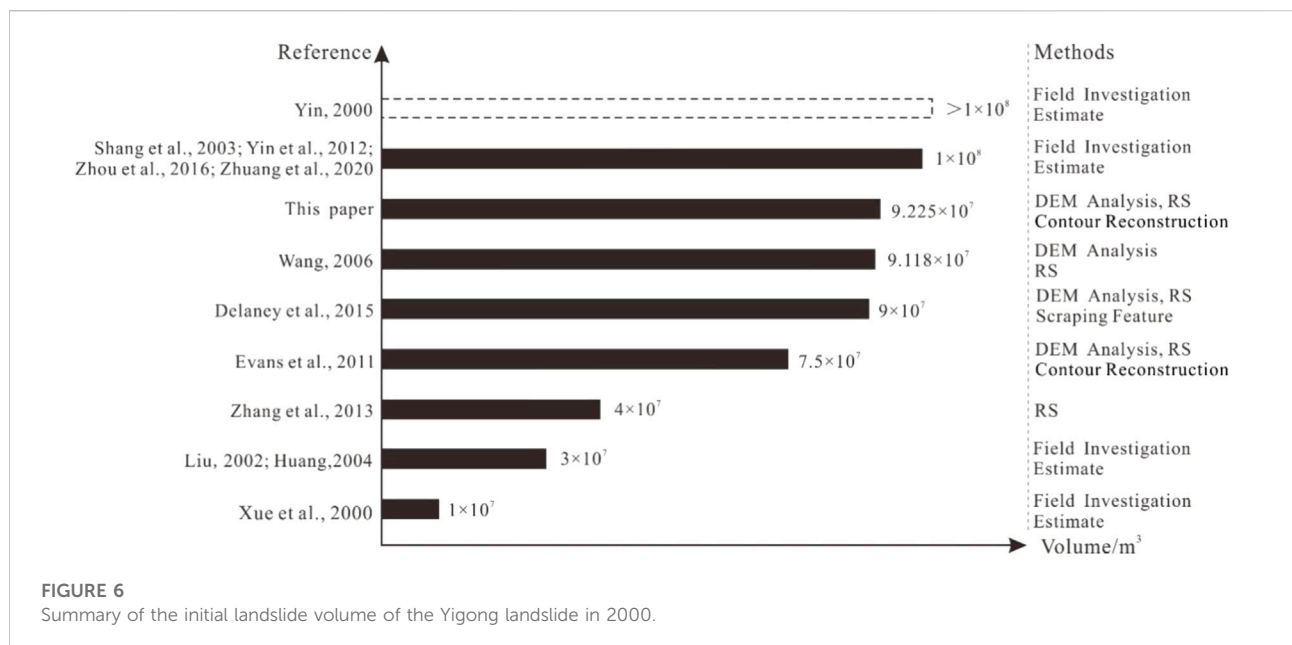
If area value is calculated according to the average thickness of the landslide deposition body obtained by Yin (2000) in the field investigation, the final deposition volume is approximately 3.06×10^8 m^3. If area value is calculated according to the average thickness of the tail of the area, the area was approximately 0.5 km^2, the average thickness of the middle was 50 m, the area was approximately 1.5 km^2, the average thickness of the tail was 65 m, the area was approximately 3.2 km^2, and the final deposition volume was approximately 2.81×10^8 m^3.

Therefore, on the basis of literature review, image interpretation before and after the landslide, and DEM calculation and analysis, this paper believes that the initial landslide volume of the Yigong landslide in 2000 is approximately 9.225×10^7 m^3, and the final deposition volume of the Yigong landslide in 2000 is approximately $2.81 \sim 3.06 \times 10^8$ m^3.

5 Initiating mechanism and sliding velocity of the Yigong landslide

5.1 Sliding velocity of the Yigong landslide

The landslide velocity is classified by the Landslide Team of the International Federation of Geosciences, and the lower limit velocity

TABLE 3 Historical studies summary of final deposition volume of the Yigong landslide in 2000.

Number	Volume/ m^3	Research methods	References
1	9.11×10^7	Remote sensing interpretation, DEM data analysis	Wang (2008)
2	$2.8\sim3.0 \times 10^8$	Field investigations	Yin (2000), Liu (2000), Zhou et al. (2000), Liu et al. (2001)
3	3.0×10^8	Field investigations, remote sensing interpretation	Zhou et al. (2001), Chai et al. (2001), Wang et al. (2002), Shang et al. (2003), Huang (2004), Xu et al. (2012)⁰
4	$>3.8 \times 10^8$	GPS field measurement, Remote sensing interpretation	Ren et al. (2001)
5	1.05×10^8	Remote sensing interpretation, DEM data analysis	Evans et al. (2011)
6	1.15×10^8	Remote sensing interpretation, DEM data analysis, GPS field mapping	Delaney et al. (2015)
7	1.67×10^8	Mass density analysis	Ekström et al. (2013)
8	1.29×10^8	Digital terrain data analysis	Liu et al. (2018)
9	$2.81\sim3.06 \times 10^8$	Comparative analysis, Remote sensing interpretation	This paper

FIGURE 7
Summary of the final deposition volume of the Yigong landslide in 2000.
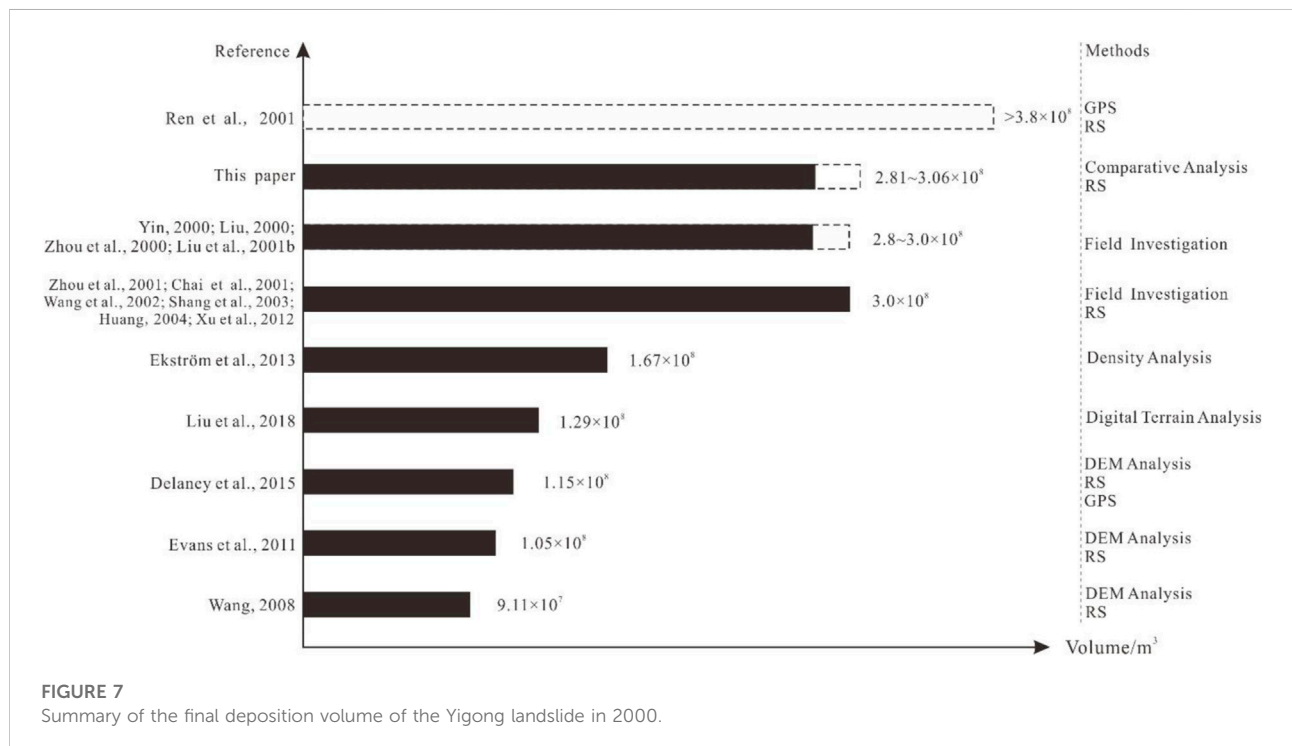
of the extremely rapid level is 5 m/s (International Union of Geological Sciences Working Group on Landslides, 1995). The velocity of the Yigong landslide far exceeded this value. The topography and geomorphology are important factors influencing the landslide velocity. The great elevation drop in Zhamunong gully gives large gravitational potential energy to the landslide body. Because the kinetic energy is higher during the collapse process, landslides have incredible velocity. The high kinetic energy is gradually depleted due to entrainment, friction and gentle terrain, and the fast movement is transformed into decelerated ddeposition.

In this study, the 2000 Yigong landslide was simulated by Massflow (Figures 4, 5). The results shown that the landslide maximum velocity is 95 m/s, the collapse velocity is approximately 48 m/s, the average velocity of the whole landslide process is approximately 45 m/s, and the average velocity of the rock debris is approximately 37 m/s. The maximum entrainment zone is located in the middle and upper part of the Zhamunong gully, and it is also the area with the highest movement velocity. The maximum thickness of the entrainment is approximately 130 m.

TABLE 4 Sliding velocity statistics research results of the Yigong landslide.

Number	Velocity (m/s)	Research methods	References
1	$V_{max} = 50$	Field investigations	Zhu et al. (2000)
2	$V_1 = 48$, $V_2 = 16$	Calculate according to seismic wave curve	Ren et al. (2001)
3	$V_3 = 37\sim39$; $V_{max} = 65$	Numerical simulation (Discrete element method)	Chai et al. (2001)
4	$V_3 = 37\sim39$	Field investigations	Liu (2002)
5	$V_3 > 14$	Field investigations	Shang et al. (2003)
6	$V_{max} > 44$	Field investigations	Huang (2004)
7	$V_{max} = 44$	Field investigations	Xu et al. (2007)
8	$V_{max} = 117$	Numerical calculation	Zhou et al. (2010)
9	$V_3 = 15.6$; $V_{max} = 129.9$	Numerical simulation (DAN software)	Delaney et al. (2015)
10	$V_{max} = 53$	Numerical simulation (PFC software)	Chen (2016)
11	$V_{max} = 110.4$	Numerical simulation (/)	Liu et al. (2018)
12	$V_1 = 90$; $V_2 = 28.5$; $V_3 = 30.12$; $V_{max} = 121$	Calculate according to seismic wave curve	Li et al. (2018)
13	$V_3 = 35$; $V_{max} = 90$	Numerical simulation (DAN software)	Dai et al. (2019), Zhuang et al. (2020)
14	$V_3 = 40$; $V_{max} = 100$	Numerical simulation (SPH method)	Dai et al. (2021)
15	$V_{max} = 138$	Numerical simulation (/)	Zhou et al. (2020)
16	$V_1 = 48$; $V_2 = 37$; $V_3 = 45$; $V_{max} = 95$	Numerical simulation (Massflow software)	This paper

SPH, smoothed particle hydrodynamics; V_1, average velocity of collapse; V_2, average velocity of debris flow; V_3, average velocity of landslide; V_{max}, Maximum velocity during landslide.

Many scholars have studied the velocity of the Yigong landslide through field investigations, seismic wave curve calculations and numerical simulations (Table 4). Statistics show that the maximum velocity of the Yigong landslide during the collapse in the slide source zone is 90 m/s. The velocity range in the state of roc debris is 16~37 m/s. The maximum velocity during the landslide process is usually located in the upper part of the fast movement and entrainment zone, the maximum velocity range is 44~138 m/s, and the average velocity range of the entire landslide process is 15.6~45 m/s.

The landslide velocity calculated by the seismic wave curve is obtained by analyzing the wave crests of the rock mass or the impact vibration of the rock debris. Therefore, it is particularly important to reasonably divide the wave crests in the motion stage and find the accurate collision point. Affected by the accuracy of the model and the simulation method, the simulation results are quite different. A more accurate velocity feature distribution requires field investigations, experiments, high-precision numerical simulations and research on better methods.
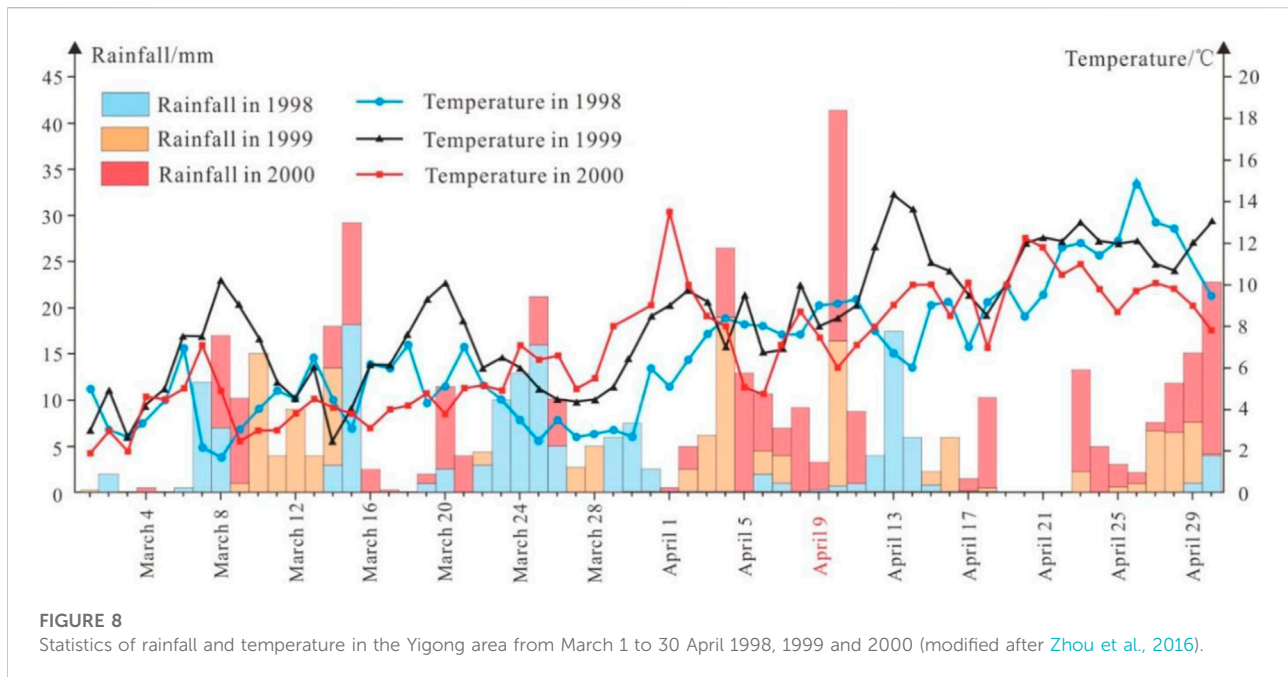
5.2 Analysis of the failure initiating mechanism of the Yigong landslide

According to the summary of the failure initiating mechanism of the Yigong landslide, the researchers' opinions are as follows: ① climate change leads to rock avalanche, ② earthquakes induce rock avalanche, ③ active faults control rock avalanche, and ④ endogenic and exogenic geological processes cause rock avalanche.

5.2.1 Climate change causes rock avalanche

The Tibetan Plateau is the earth's "third pole", as well as the initiation, sensitive and key areas of global climate change response. Temperature data and model predictions from 1970 to 2000 show that the Tibetan Plateau will continue to heat up (Yao et al., 1994, 2000; Wang et al., 1996; Li et al., 2006; Hao et al., 2013; Li et al., 2021). The rise of the snow line and melting of snow and ice will increase the probability of geological hazards, such as collapses, landslide and debris flows, and promote the extension and conversion of the geological hazard chain (Shang et al., 2003; Mcguire et al., 2010; Cui et al., 2014). The occurrence of the Yigong landslide in 2000 is related to climate change. Guo (2015) combined remote sensing images, meteorology, and Moderate Resolution Imaging Spectroradiometer (MODIS) data to analyze the ice and snow thawing range, air temperature and ground temperature and concluded that the air temperature had risen above 0°C 1 month before the Yigong landslide occurred. Two weeks before the landslide, the center of the landslide body easily absorbed heat due to the fragmentation of the rock mass. The endothermic causes the temperature at the location of the landslide body to be higher than the surrounding pixels by 2~8°C. The slide source zone showing a high temperature center. When the ground temperature reached 5°C on March 28, the surrounding area of the slide source zone began to thaw. Zhou et al. (2016) compared the temperature in the Yigong area from

FIGURE 8
Statistics of rainfall and temperature in the Yigong area from March 1 to 30 April 1998, 1999 and 2000 (modified after Zhou et al., 2016).

March 1 to May 4 in 1998, 1999, and 2000 (Figure 8), and concluded that there was no significant difference in temperature changes in the 3 years. However, the temperature rise on 1 April 2000, might had an impact on the landslide. Finally, the warmer temperatures led to snow melt and the continuous precipitation was 50 mm in the area from 1st April to 9th April 2000, which is 50%–90% higher than the average value in the same period. The water infiltrated into the joints and fissures of the rock mass in the source zone. It led to the rise of pore water pressure and weaken the rock mass structural surface, which finally induced the instability of the wedge-shaped body (Liu, 2000; Wan, 2000; Yin, 2000; Zhou et al., 2000; Liu et al., 2001; Ren et al., 2001; Shang et al., 2003; Huang, 2004; Xu et al., 2007; Xu et al., 2012; Zhang et al., 2013).
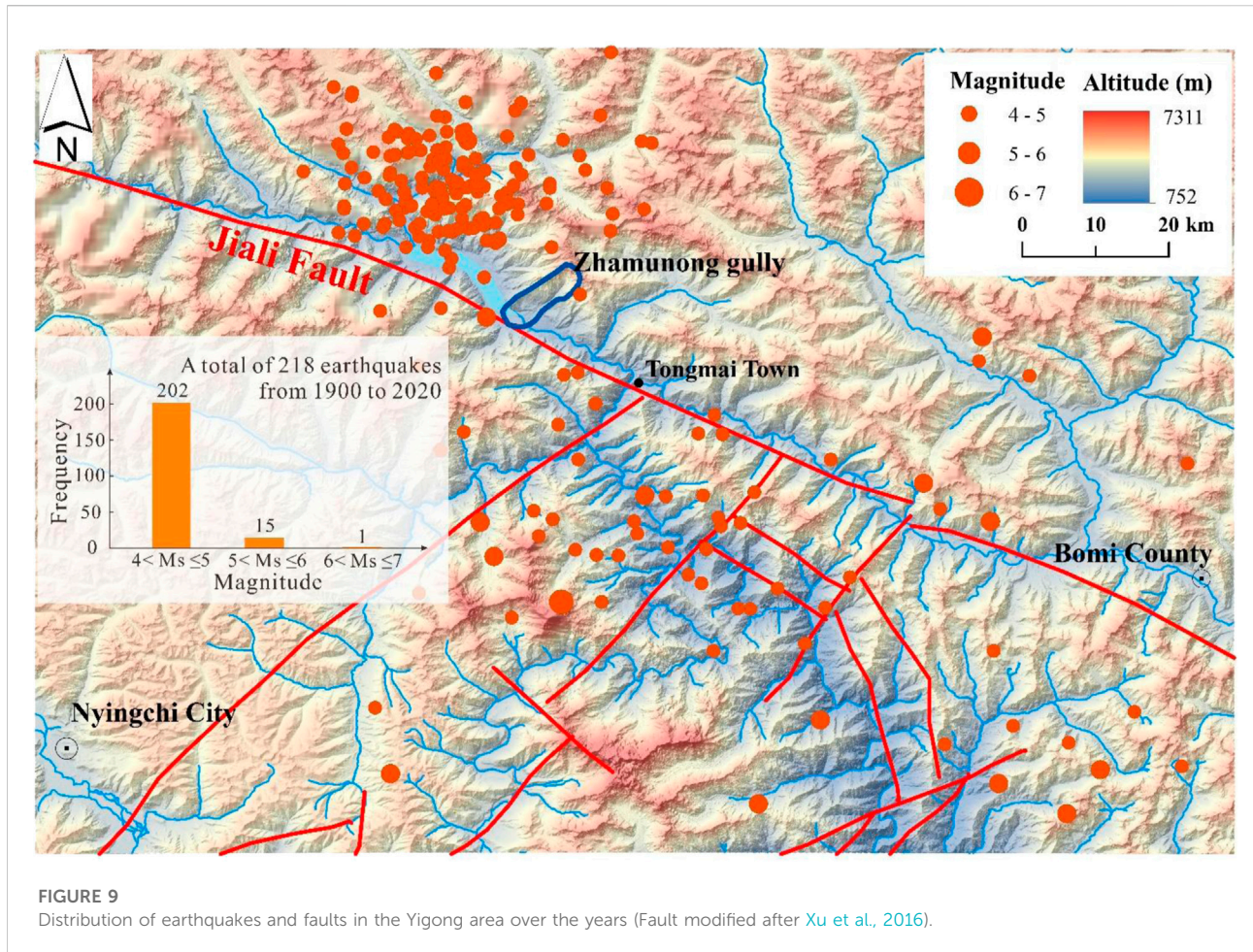
5.2.2 Active faults control rock avalanche

Faults are development in the Zhamunong gully (Figure 4). Large area that are affected by theJiali fault zone. The creep and stick-slip effects of the faults control the topography, rock mass structure and slope stress field of the large area. Therefore, geological hazards in this area are extremely developed (Zhang et al., 2016). For example, the Xianshuihe fault zone in western Sichuan has an obvious controlling effect on geological hazards. Approximately 67.5% of geological hazards develop within 1.5 km away from the fault zone. The sliding directions of landslides are mostly perpendicular to the fault strike (Guo et al., 2015). Zhamunong gully is greatly affected by the Danen-Zep fault and the Dade-Aniza secondary fault (Figure 9). The rock mass

structure near the fault is broken, and the rock mass is easily unstable under the exogenic geological processes. Lu et al. (2000) comprehensively analyzed the influence of climate, topography, and the geological structure on the Yigong landslide and believed that the geological structure is one of the main factors in landslide formation. Liu et al. (2000) also believed that the geological structure was one of the main factors for the landslide, and the Zhamunong gully formed a concave terrain under the influence of the Azha-Yigong fault and the Shencuo Jiuzila-Langxiama fault. The tectonic movement led to the formation of dense joints and fissure development zones. These zones produced many collapse deposits under weathering. Once it reached the limit equilibrium state, it would have induced large-scale landslides.

5.2.3 Earthquakes induce rock avalanche

Earthquakes are important factors that induce geological hazards. For example, the Wenchuan Ms8.0 earthquake in 2008 triggered more than 15,000 landslides, collapses and debris flows. The post-earthquake caused more than 10,000 hidden danger points of geological hazards (Yin, 2008). The Ms6.5 Ludian earthquake in 2014 triggered approximately 10,559 landslides (Wu, 2018).

The Yigong landslide is located in the eastern Himalaya tectonic junction area. This area is located on the front edge of the Indian Ocean plate subducting underneath the Asian-European plate. Frequent seismic activity occurs and near-upright and steep slopes develop. The V-shaped alpine canyon not only amplifies seismic waves but also intensifies hazard effects (Quan et al., 2021). According to statistics, more than

FIGURE 9
Distribution of earthquakes and faults in the Yigong area over the years (Fault modified after Xu et al., 2016).

200 earthquakes have occurred in the Yigong landslide region from 1900 to 2020, among which are small and medium earthquakes with magnitudes of Ms 4.0–5.0. It is worth noting that most earthquakes are distributed within 35 km of the northwest side of Zhamunong gully, and more than 100 earthquakes could affect the Zhamunong gully (Figure 9). Most of earthquakes are small and medium earthquakes (Shao, 2009; Li et al., 2018). Frequent small and medium earthquakes would increase the fragility of the rock mass and become the factor triggering rock mass instability.

Li et al. (2018) analyzed earthquakes, temperature data and precipitation in the first 2 months after the landslide occurred. The granite body in the source zone that experienced long-term action was in a state of limited equilibrium and had been damaged. Finally, affected by the Ms4.8 earthquake in the Nyingchi area at 8:00:09 a.m. on April 9th, 13 km from Zhamunong gully, the Yigong landslide occurred at 8:00:11.95 a.m. Based on the seismic acceleration and the coupled spatiotemporal analysis of the Yigong landslide, the earthquake was likely the key factor that induced the Yigong landslide.

5.2.4 Endogenic and exogenic geological processes cause rock avalanche

Endogenic geological processes, such as earthquakes, crustal uplift, and fault activity, and exogenic geological processes, such as weathering, denudation, transport, and deposition, cause stress release or structural damage. Both endogenic and exogenic geological processes directly or indirectly affect the formation of landslides (Wang, 2002; Li et al., 2008). Lv J. L. et al. (2003) believed that the rock mass structure was extremely fragmented due to linear structural cutting and freeze-thaw weathering in the Zhamunong gully area, and active faults and earthquakes aggravated the weakening of the rock mass structure and the accumulation of landslide material. A large amount of ice and snow accumulated in the source area and increased the weight of the slope. Affected by the seasonal climate, a large amount of ice and snow melted water, and precipitation infiltrated the broken rock mass, resulting in the weakening of the structural surface and an increase in the pore water pressure. Therefore, the combination of endogenic and exogenic geological processes led to the Yigong landslide. Zhou et al. (2016) believed that the Yigong landslide was caused by the

coupling of long-term evolution and short-term effects. Long-term, the loading and unloading of ice and snow on the rock mass, seasonality, and solar freeze-thaw cycles gradually reduced the mechanical properties of the rock mass and caused the joints and fissures to penetrate together. Short-term, the increase in temperature before the Yigong landslide accelerated the melting of ice and snow, and the continuous heavy rain caused the rise in the pore pressure of the rock mass and the mechanical strength of the rock mass to decrease sharply. Wen et al. (2004) counted 70 large-scale landslides in China since 1900 and concluded that their genetic mechanisms are very complicated. Structural conditions, geological conditions, lithology, and topography are factors influencing large-scale landslides. The triggering factors of large-scale landslides are usually rainfall, earthquakes, slope top loads and snowmelt.

In summary, the failure initiating mechanism of the Yigong landslide can be revealed as follows. It is controlled by endogenic and exogenic geological processes and is triggered by short-term effects, such as seasonal changes in climate, heavy rainfall, and strong earthquakes during the long-term creep process of the rock mass. Long-term factors that control the creep of rock masses are as follows: ① Seismic action. More than 100 earthquakes affected the Zhamunong gully region from 1900 to 2020, mainly small and medium earthquakes with values of Ms 4.0~5.0. The frequent earthquakes caused rock mass damage. ② Fault creep effect. The strike-slip rate of the central part of the Jiali fault zone is 1.3 mm/a, and the extrusion rate is 2.9 mm/a, which indicates a creeping state (Tang et al., 2010). It controls the topography, rock mass structure and slope stress in this area. ③ Freeze-thaw and loading and unloading cycles. The altitude of the rear edge of Zhamunong gully is more than 5,000 m, and the gully has experienced a cycle of snowfall and snowmelt for many years. The melting cycle and loading and unloading effects can led to the continuous expansion of the joints and fissures of the bedrock source zone. ④ The dry-wet cycle effect. The unique geographical location of Zhamunong gully brings abundant precipitation, which makes the regional dry-wet cycle extremely strong and continuously weakens the rock mass strength. These four factors mentioned above control the creep of the rock mass long-term. In the short-term, from April 1st to 9 April 2000, the Zhamunong gully area accumulated more than 50 mm of precipitation, the regional temperature rose beginning on March 27, and the temperature on April 1st reached the highest value in 3 years (Figure 8). The effects of snowmelt and rainfall were both large during this period. During this period, the rock mass in the landslide source zone of Zhamunong gully was close to the limit equilibrium state. When ice and snow melt water and the continuous heavy rainfall seeped into the joints and fissures of the rock mass, the structural surface strength of the rock mass decreased, and the pore water pressure increased. Finally, the rock mass broke the limit and broke the restraint of the locked section, resulting in the Yigong landslide.

6 Research on the Yigong landslide-river blockage-dam breakage hazard chain

The dam formed by the Yigong landslide in 2000, with bottom widths of 2,200~2,500 m, an axis length of approximately 1,000 m, a plane area of approximately 2.5 km^2, and a maximum storage capacity of 288×10^8 m^3 (Yin et al., 2000). Some scholars believe that the maximum storage capacity is 201.5×10^8 m^3 (Delaney et al., 2015). After the blockage of the Yigong Zangbo River, the plan of opening a canal and drainage was adopted to dredge the river. Construction began on 3 May 2000 and was completed on June 4th. The canal is a trapezoidal section, with a bottom width of 30 m, a canal depth of 20 m, and lengths of approximately 600~1,000 m. The channel began to discharge on June 8th, the dam began to collapse at 20:00 on June 10th, and it basically returned to its original state at 19:00 on June 11th. During the discharge process, the instantaneous maximum flow appeared at 2:00 on June 11th, and the water level downstream of the dam body rose by at least 48.2 m. The flow at the downstream Tongmai Bridge reached 12×10^4 m^3/s, and the water level of the river was approximately 41.77 m and 32 m above the bridge deck. On June 12th, approximately 30×10^8 m^3 of the reservoir water in Yigong Lake was completely discharged (Lu et al., 2000; Shang et al., 2003). The bursting floods washed away bridges and roads and induced secondary hazards, causing massive harm to the downstream areas.

6.1 Volume of the Yigong landslide dammed lake

At present, the dammed lake formed by the Yigong landslide and blocking the river is generally considered to have a discharge volume of approximately 30×10^8 m^3 (Lu et al., 2000; Yin et al., 2000; Shang et al., 2003). The area and volume of the dammed lake continued to expand after the blocking of the river. The extent of expansion was closely related to climatic factors, upstream flow. This paper considers the volume of the dammed lake obtained by methods such as measured data and digital elevation model (DEM) data (Table 5). In addition, some scholars have used numerical simulations, empirical formulas, and other methods to analyze the volume of the Yigong dammed lake, the outburst flow, and the impact on the downstream flow and river erosion (Lu et al., 2000; Yin et al., 2000; Shang et al., 2003; Zhuang et al., 2021). By comparison (Figure 10), the trend of the area and volume of the dammed lake calculated from the DEM data are similar, but there is a certain gap in the measured results. Moreover, there are also differences in the area and water volume assessments at the time of the burst. Wang et al. (2002), Lv J. T. et al. (2003) and Wang et al. (2005) found that the water surface elevation, area, and volume at the time of the collapse were 2,244 m, 52.855 km^2 and 23.29×10^8 m^3,

TABLE 5 The statistical table of lake volume of the Yigong landslide dam in 2000.

Time	Water surface elevation/m	Lake area/km²	Water volume × 10⁸/m³	Research methods	References
Before damming	—	15.000	0.70	Field measurements	Yin Y. P. (2000)
24th, May		44.400	10.70	Measured by the ADCP method	Zhou G. Y. et al. (2000)
8th, June		50.000	31.44	Field measurements	Lu X. Y. et al. (2000)
8th, April		19.900	—	Remote sensing interpretation	Wang Z. H. et al. (2001)
4th, May		33.700			
9th, May		37.300			
20th, May		43.600			
13th, April	2,214	18.909	1.55	Remote sensing interpretation; DEM data analysis	Wang et al. (2002), Wang Z. H. (2005)
4th, May	2,225	33.659	5.84		
9th, May	2,228	36.320	7.76		
12th, May	2,229	37.979	8.41		
20th, May	2,234	43.121	13.05		
10th, June	2,244	52.855	23.29		
17th, June	2,209	9.280	0.43		
—	2,220	24.072	1.75	Remote sensing interpretation; DEM data analysis	Delaney et al. (2015)
	2,225	28.010	3.13		
	2,230	31.939	4.69		
	2,240	38.241	8.51		
	2,250	43.371	12.87		
	2,255	45.251	15.11		
	2,260	47.064	17.59		
	2,265	48.926	20.15		
	2,270	50.578	22.80		
	2,280	53.272	28.29		

ADCP (Acoustic Doppler Current Profilers).

respectively. Delaney et al. (2015) believed that they were 2,265 m, 48.926 km² and 20.15 × 10⁸ m³, respectively. At present, it is believed that the volume of the Yigong landslide dammed lake was approximately 20~30 × 10⁸ m³ before the burst. Precise calculation of the volume of the Yigong dammed lake should integrate with field investigations and mapping data, combine with high-precision historical remote sensing images, and correct the elevation value interpreted by the remote sensing images.

6.2 Yigong dam failure mechanism

Lu et al. (2000) believed that sandy loam containing gravel was mainly in the vicinity of the discharge channel, with a high content of silt and fine sand, a loose structure, and poor scour resistance. Liu et al. (2001) analyzed three aspects of the failure mechanism: the material composition of the dam body, the shape of the longitudinal section of the channel, and the water level due to continuous rainfall. First, the material composition of each part of the channel section is different (Table 6). The sandy loam contains broken and lumpy stones. Because the particle sizes of the broken and lumpy stones are different, a loose structure is easily formed after flow and deposition, and the sandy loam particles are relatively fine and easily removed by the scouring of the flowing water, so the overall anti-scour of the dam body is less capable. Second, the water inlet of the longitudinal section of the diversion channel is low, the middle is high, the tail of the channel is low and there is no slope. So the drainage cannot be smoothly drained. This process results in the soaking of the water inlet and the expansion of the width by approximately 350 m. From the middle to the tail of the channel, due to the large drop, the flow velocity of the water increases. The tail of the channel cut upstream and downward and two sides of the channel collapse inward. Finally, the upper reaches of Yigong Lake experienced rain for several days from June 8th to 10th, and the amount of water entering the reservoir was greater than the amount of water discharged. Therefore, the water level of the reservoir rose rapidly, resulting in a high head difference and causing the dam to burst. Shang et al. (2003) believed that rainfall
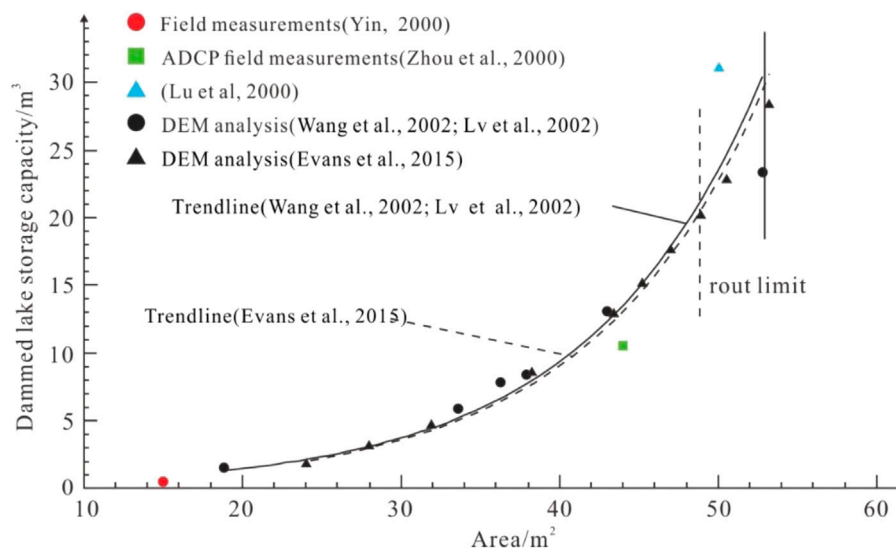
FIGURE 10
Comparison of the area and volume of the Yigong dammed lake.

and meltwater entered the dammed lake. Channel diversion was completed too late. As a result, the reservoir water exceeded the water volume predicted before diversion, resulting in a rapid rise in the water level and the occurrence of piping and seepage. In addition, loose dam accumulation also contributes to dam failure and flooding. By analyzing the dam material and material particle classification curve of the dam in 2000, Li et al. (2017) believed that the rock blocks of the dam body were not only poorly rounded and had different particle sizes but also had a high clay content. Thus, the material was a typical broadly graded soil with a high clay content. This kind of dam usually reduces the structural strength greatly with increasing water level, and it is very easy to cause flood top failure. The stability of the widely graded dam body is affected by the material composition and structure type of the dam body, the cross-sectional shape of the drainage channel, and the water level differences of the river and lake, which are prone to damage in the form of seepage effects and immersion collapse. These factors should be fully considered during drainage.

6.3 Characteristics of the dammed lake-dam break hazard chain

Floods formed in the alpine and canyon areas, the complex terrain makes it generates strong hydrodynamic effects, and the shear stress on the riverbed. Especially in steep canyons and areas where river valleys shrink and narrow, floods can remove several meters of boulders and have a strong ability to transform topography (Turzewski et al., 2019). The Yigong long-runout landslide has the typical geological characteristics of a collapse-

landslide-debris flow-river blockage-dam break-flood-secondary hazard chain. The dam break-flood hazard chain has far-reaching impacts and causes great harm. It not only destroyed downstream bridges, roads and infrastructure but also induced many secondary hazards (Figure 11). Wan (2000) and Zhu et al. (2001) analyzed and compared multiperiod remote sensing data. They believed that the flood produced by the dam failure caused approximately 25 new landslides of different scales downstream, and the original forests and grasslands were covered with new riverbed beach. Liu et al. (2002) and Lv J. L. et al. (2003) believed that the Yigong landslide dam break hazard chain affected an area of approximately 450 km downstream along the river, and the slope toe instability phenomenon occurred due to flood erosion of hundreds of kilometers in the valley. Some river valleys have changed from V-shaped to U-shaped. The bank slopes are steeper. In addition, some river valleys have become shallow traction landslide belts. There are at least 15 landslides and collapses in the affected area. Their volume is mostly between hundreds of m^3 and several m^3. Through remote sensing interpretation and other methods, Wang (2005) and Xu et al. (2012) revealed that approximately 35 slope surface slumps, shallow landslides and slope debris flows were triggered on both sides of the main river channel 120 km downstream. The largest debris flow area on the slope is 0.8 km^2. The river channel has been widened by more than 2 to 10 times, and the affected distance is more than 120 km. Delaney et al. (2015) believed that the Yigong landslide dam break-flood hazard chain destroyed at least six bridges. The affected area extended to Brahmaputra, northeastern India, 500 km downstream of the landslide location. At the same time, the Pasighat gauging monitoring station

TABLE 6 Material composition table of the Yigong landslide dam body in 2000.

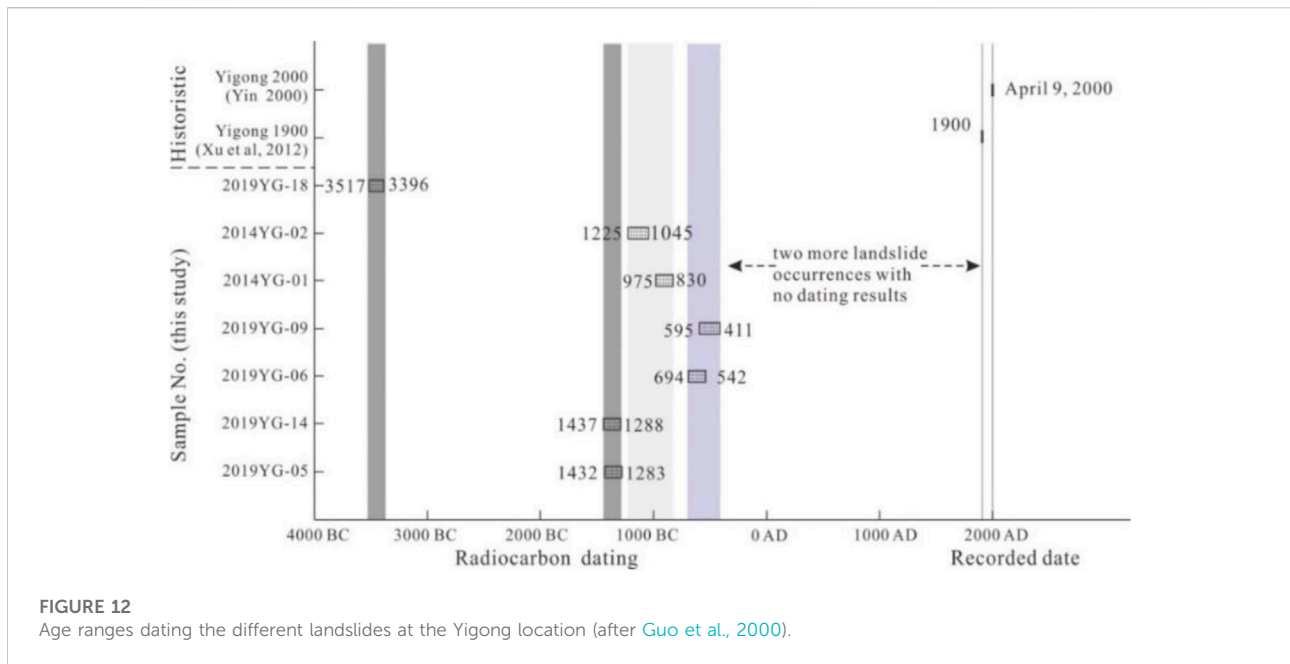|	Tail of drainage channel	Middle of drainage channel	Aqueduct entrance
Channel elevation	Low	High	Low
Material composition	Gray-white colored sandy loam contains crushed stones, lump stones and large 3stones. The content of crushed and block stone content 30~40%. The diameter of the blocks is generally 3~20 cm, the large ones are 1~5 cm, and some are >10 cm	Crushed and lump sandy loam soil, in which the content of crushed and lumpy block is 50~60%	The sandy loam contains crushed stone and block stone. The composition of crushed stone and block stone is mainly marble, quartzite and granite. The content of crushed and block stone is 50~60%

FIGURE 11
The Yigong landslide hazard chain in 2000 (a and b maps based on Google Earth; **(A)** Influence area of the Yigong landslide—dam break in 2000;
(B) The Yigong landslide and Yigong Lake; **(C)** Flood level of the Tongmai Bridge in 2000; **(D)** Elevation diagram of the new Tongmai Bridge).

FIGURE 12
Age ranges dating the different landslides at the Yigong location (after Guo et al., 2000).

TABLE 7 Characteristics of potential collapse landslide in Zhamunong gully (modified after Li et al., 2017).

Number	Width/m	Average avalanche area/m^2	Volume $\times$ 10^8/m^3
BH01	935.30	100,314.00	0.94
BH02	822.07	111,879.50	0.92

located at 462 km recorded the water level rise at 5.5 m (Figure 11A). The dam break-flood hazard chain has a far-reaching impact, which not only induces secondary hazards but also seriously harms engineering facilities along the way. The research content focuses on the number of secondary hazards and the scope of flooding. The research methods are mostly remote sensing interpretation and monitoring station data analysis.

7 Research progress on the recurrence cycle of the Yigong long run-out landslide

The landslide recurrence cycle refers to the repeated occurrence of landslides of a certain scale at the original site of the landslide under relatively stable environmental conditions, and the occurrence time of each landslide has a certain periodicity. The recurrence period of landslides has a certain relationship with the erosion and accumulation rate caused by climate, earthquakes, rivers. Shang et al. (2003) deemed that the Yigong landslide material accumulation rate was approximately

0.149 m^3/year/m^2. When the material accumulates to the limit, it is triggered by a certain influence. After the Yigong landslide in 2000, under the influence of regional climate, structure, and other factors, Zhamunong gully entered a new accumulation range of material and energy. When the boundary threshold is exceeded, landslides and river blockages are very likely to occur again.

Guo et al. (2020) revealed that the Yigong landslide has a periodic long run-out landslide-damage Yigong Zangbo dam break hazard chain recurrence pattern through field investigations, geological profile measurements, fine stratigraphic determination and ^{14}C dating in the Yigong landslide accumulation area. Guo et al. (2020) believed that in the past 5,500 years, at least 8 long run-out landslide events occurred in the source area of the Yigong landslide in 2000, namely, 3500 BC, 1300 BC, and 1000 BC, 600 BC, 1900 and 2000 landslide events, respectively, and two landslide events from 600 BC to 1900 that lack dating data. The results reveal that the landslide area has a recurrence cycle of approximately 200–500 years (Figure 12). Considering the eroded deposits of later landslide events and the incomplete records of landslide-damage events, there may be a century-scale recurrence cycle of large-scale long run-out landslides in the Yigong area.
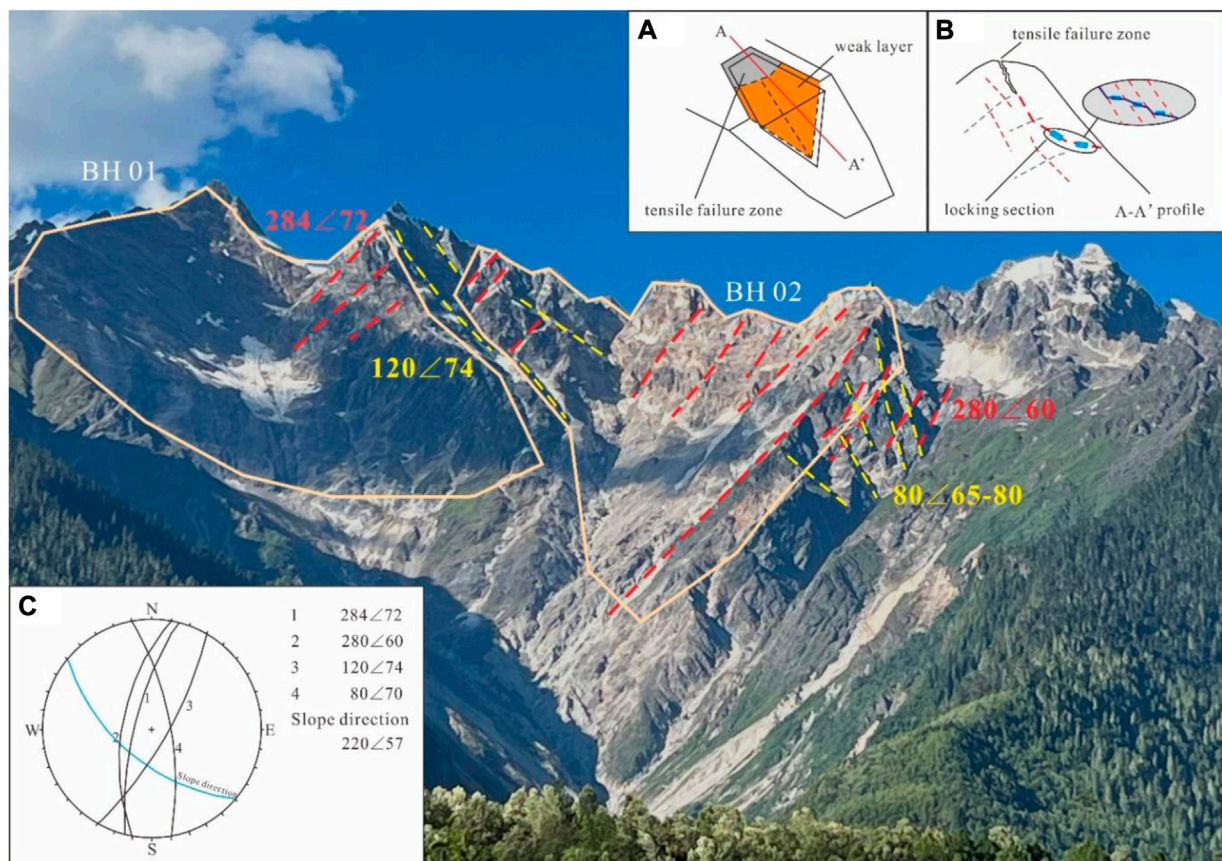
FIGURE 13
Structural characteristics of rock mass in the source zone of the Yigong landslide (mirror to NE) [**(A)** wedge failure mode; **(B)** locking section failure mode; **(C)** stereographic analysis].

Taking the Yigong landslide as an example, it has a periodic initiating mechanism with characteristics of head-cut and recurrence. Under relatively stable environmental conditions, after long-term effects such as climate, micro seismicity, and fracture creep, landslide materials continue to accumulate, and rock mass damage also continue to intensify. Without the influence of emergencies, the limit will reach within a certain period. The recurrence period of such landslides can generally be identified by methods such as remote sensing images or stratigraphic determination of deposition zone.

8 Research prospects

8.1 Stability discussion of the Yigong long-runout landslide source zone

There is still a greater risk at the rear edge of Zhamunong gully. Lv J. L. et al. (2003) believed that 1×10^7 m^3 of loose matter remains in the Zhamunong gully. It is currently in a new cycle of deposition of matter and energy after the Yigong landslide in 2000. Through remote sensing image interpretation, Zhu et al. (2015) found that the total volume of loose deposits and potentially unstable rock mass in the source zone of Zhamunong gully reached more than 1.6×10^8 m^3. Under the influence of heavy rainfall, melting ice and snow, and avalanches, there is the possibility to produce large landslide. Through engineering geological analysis methods and field surveys, Li et al. (2017) believed that there are still two large potential dangerous rock mass at the rear edge of Zhamunong gully, of which the BH01 is 0.94×10^8 m^3 and 0.92×10^8 m^3 for BH02 (Table 7; Figure 13). The assessment result used MacCormack-TVD method suggests the collapses of BH01 and BH02 will cause the Yigong Zangbo river blockage. Liu et al. (2020) analyzed the response characteristics of the mountains in the Yigong area to seismic waves and used FLAC^{3D} software to study the stability of dangerous rock mass. Under the action of strong near-field earthquakes, the dangerous rock mass will unstable.

Structural planes develop in hard-extremely hard rock masses. The rock mass between the joints and fissures is obliquely cut and penetrated at the weakest part, causing the locking section to be sheared step by step to form a landslide (Bunkholt et al., 2012; Stead et al., 2013; Huang et al., 2015). The lithology of the slide source area is granite. The field investigation and data collection show that the rock mass in the Zhamunon gully slide source zone of the Yigong landslide is affected by three groups of dominant joint control, NW (280 < 60, 284 < 72, 328 < 45), NE (80 < 65-80, 64 < 32, 58 < 32, 48 < 59) and SE (120 < 74, 94 < 57). The joints in the NW and NE directions controlled the development of the wedge-shaped body in the Yigong landslide in 2000 (Figure 13). The comprehensive analysis shows that the failure mode of the wedge in 2000 was creep-tension-shear. Li et al. (2018) also made the same analysis, and he believed that the locking section is distributed in the middle part. Firstly, the trailing edge is along the slope of the joint, which is fractured and penetrated under the action of pore water pressure, frost heave force and gravity. Then the sliding stress is borne by the locking section of the shear surface (Figure 13). When the stress accumulation in the creeping process exceeds the bearing limit of the locking section, the elastic impulse effect occurs (Hu et al., 1992; Cheng et al., 2000). Then the locking section suddenly cuts off and slides at a high velocity. There are still two potential risk areas, BH01 and BH02. Wang et al. (2021) believed that there was big deformation in the BH02 zone by InSAR deformation analysis. Combined with InSAR and engineering geological analysis, it is shown that the eastern rock mass of BH01, the western rock mass of BH02 and the eastern rock mass of BH02 are dangerous. The dangerous rock mass has the possibility of instability under the effect of earthquakes, freeze-thaw and rainfall.

As a result, it suggested to assess the danger of Zhamunong gully, and distinguish the scale, stability and disaster impact in the landslide source zone. It is also necessary to carry out research on the weakening mechanism of granite body strength in the Yigong area to reveal such rock masses in alpine and alpine regions.

8.2 Study on the influence range of the Yigong landslide-dam blockage-dam break hazard chain

In 2000, the hazard chain induced by the Yigong landslide had a large impact area, which caused great harm to infrastructure, such as roads and bridges, and downstream urban residents. At present, the Yigong Zangbo Bridge and other bridges in the construction plan are located within the dam-flood impact range. If the potential dangerous rock mass block the river, the induced hazard chain will lead to the

destruction of roads and bridges and the interruption of railway.

Therefore, it is necessary to accurately analyze and calculate the storage capacity of Yigong Lake, the flood level of the dam break after the landslide blockage by the potential landslide, and the impact range of the hazard chain. The commonly used methods for research on the range of the hazard chain mainly include field sign identification, remote sensing image interpretation, numerical simulation, InSAR monitoring and monitoring station records. The current research focuses on the scale of secondary hazards induced by dam break floods.

However, few studies focus on the dynamic characteristics of dam break floods, the mechanism of inducing hazards, and the regional characteristics of secondary hazards. These research can strengthen to help support the design and planning of railway lines and bridges, formulate hazard prevention and mitigation measures, and reduce the hazards risk.

8.3 Research on the remote monitoring and early warning of landslides in extremely high mountain areas

The long-runout landslides in extremely high mountain areas, such as the Yigong landslide, have the characteristics of beyond visual range concealment, high altitude start and short process time. It is usually located in the middle and upper parts of the steep slope in the V-shaped valley area, and the altitude can over 4,000 m. The slide source zone is usually covered by ice, snow or vegetation. The landslide often ignored because it is difficult to conduct the investigation manually. Therefore, the traditional manual investigation method is no longer applicable to the concealment of the long-runout landslides beyond the visual range. Xu et al. (2019) proposed an integrated air-space-ground three-inspection system that can effectively carry out the early identification of long-runout landslides. They first used optical remote sensing and synthetic aperture radar interferometry (InSAR) technology to identify and survey large-scale disasters from a "deep space" macro perspective. Then based on airborne light detection and ranging (LiDAR) and drone photography technology, a detailed investigation of some major hidden danger areas or major hidden dangers is carried out from the "sky" sub-macro perspective. Finally, according to professional field surveys and slope monitoring methods, ground surveys of geological hazards, such as landslides, collapses and debris flow with major hidden dangers were carried out. Landslides in extremely high mountain areas have the characteristics of complex topography, geomorphology, geological background, and genetic mechanisms. Studies such as multi-means investigations based on modern technology coordination, key monitoring of high-risk individuals, early warning of multisource coupled factor indicators, and emergency response to major

geological hazards are critical for prevention and control (Xu, 2020).

9 Conclusion

The long-runout landslide formation mechanism is very complex, since the Yigong long-runout landslide's occurrence in 2000, many scholars have carried out a lot of research on the distributing characteristics and formation mechanism. This paper summarizes and analyzes the research status of Yigong landslides, the following conclusions and understandings are obtained.

First, based on remote sensing interpretation, high-precision DEM data and field investigations, it is revealed that the volume of the Yigong landslide source zone in 2000 is approximately $9,225 \times 10^4 \, m^3$, and the volumes of deposition is approximately $2.81\sim3.06 \times 10^8 \, m^3$.

Second, the maximum velocity of the landslide is located in the upper part of the fast movement and entrainment zone. The maximum velocity range of the landslide is 44~138 m/s, and the average velocity range of the whole process of the landslide are 15.6~45 m/s. The velocity range of the rock debris is 16~37 m/s. There are differences in the understanding of the distribution characteristics of the landslide velocity, which need further study based on high-resolution topographic data, field investigation and analysis, seismic wave curves and tests.

Third, the initiating mechanism of the Yigong long-runout landslide are jointly controlled by endogenic and exogenic geological processes. The long-term creep of the rock mass aggravates the occurrence of landslide. Long-term impacts including the small and medium earthquakes, freeze-thaw cycles, dry-wet cycles, loading and unloading cycles. In addition, the landslide was triggered by short-term impacts, such as rainfall, melting ice and snow. The processes analysis will be useful for research on the stability analysis and instability trend of rock mass in alpine regions.

Fourth, the Yigong landslide has a periodic initiating mechanism with characteristics of head-cut and recurrence, and its recurrence period may be on the scale of hundreds of years. There are two potentially dangerous rock masses with a single volume of nearly 10 million cubic meters. The landslide blockage-dam break-flood hazard chain might occur again.

Fifth, it is suggested to carry out InSAR deformation monitoring, rock damage pattern and stability assessment and landslide-dam blockage-dam break hazard chain effect research on the dangerous rock mass in Zhamunong gully. (Huang et al., 2017; Lin et al., 2022).

Data availability statement

The original contributions presented in the study are included in the article/Supplementary Material, further inquiries can be directed to the corresponding author.

Author contributions

CG and HY framed the study plan and wrote the paper. HY, ZY, and RW carried out subsequent field investigations and landslide simulations, HY and YY drew the figures. Correspondence and requests for materials could be addressed to HY (yh_313@126.com).

Funding

Acknowledgments

Conflict of interest

The authors declare that the research was conducted in the absence of any commercial or financial relationships that could be construed as a potential conflict of interest.

Publisher's note

All claims expressed in this article are solely those of the authors and do not necessarily represent those of their affiliated organizations, or those of the publisher, the editors and the reviewers. Any product that may be evaluated in this article, or claim that may be made by its manufacturer, is not guaranteed or endorsed by the publisher.

References

Bunkholt, H., Redfield, T. F., Osmundsen, P. T., Oppikofer, T., Hermanns, R. L., and Dehls, J. F. (2012). *Landslides and engineered slopes: Protecting society through improved understanding*. Boca Raton, FL, USA: CRC Press, 855–861. Available at: https://www.researchgate.net/publication/265650479_Landslide_processes_in_hard_rock_in_Troms_Norway.

Chai, H. J., Wang, S. T., Xu, Q., Huang, R. Q., and Fan, X. D. (2001). Numerical simulation on overall process of Yigong slump at Bomi, Tibet. *Geol. Hazards Environ. Prot.* 12 (2), 1–3. (in Chinese with English abstract). doi:10.5194/nhess-2020-289

Chen, L. Z. (2016). *Three-dimensional numerical simulation of Yigong rock avalanche using particle flow code*. Chengdu: Southwest Jiaotong University. (in Chinese with English abstract).

Cheng, Q. G., Hu, H. T., Hu, G. T., and Peng, J. B. (2000). A study of complex accelerated dynamics mechanism of highvelocity landslide by elastic rocky impulse and peak-residual strength drop. *Chin. J. Rock Mech. Eng.* (2), 173–176. (in Chinese with English abstract). doi:10.3321/j.issn:1000-6915.2000.02.010

Cheng, Q. G., Zhang, Z. Y., and Huang, R. Q. (2007). Study on dynamics of rock avalanches state of the art report. *J. Mt. Sci.* 25 (1), 72–84. (in Chinese with English abstract). doi:10.3969/j.issn.1008-278

Clague, J. J., and Evans, S. G. (1987). Canadian geographer/le géographe Canadian. *Can. Geogr.* 31 (3), 278–282. doi:10.1111/j.1541-0064.1987.tb01243.x

Cui, P., Chen, R., Xiang, L. Z., and Su, F. H. (2014). Risk analysis of mountain hazards in Tibetan plateau under global warming. *Clim. Change Res.* 10 (2), 103–109. doi:10.3969/j.issn.1673-1719.2014.02.004

Dai, X. J., Yin, Y. P., and Xing, A. G. (2019). Simulation and dynamic analysis of Yigong rockslide-debris avalanche-dam breaking disaster chain. *Chin. J. Geol. Hazards Prev.* 30 (5), 1–8. (in Chinese with English abstract). doi:10.16031/j.cnki.issn.1003-8035.2019.05.01

Dai, Z. L., Xu, K., Wang, F. W., Yang, H., and Qin, S. (2021). Numerical investigation on the kinetic characteristics of the Yigong debris flow in Tibet, China. *Water* 13 (8), 1076. doi:10.3390/w13081076

Delaney, K. B., and Evans, S. G. (2015). The 2000 Yigong landslide (Tibetan plateau), rockslide-dammed lake and outburst flood: Review, remote sensing analysis, and process modelling. *Geomorphology* 246, 377–393. doi:10.1016/j.geomorph.2015.06.020

Ekstrom, G., and Stark, C. P. (2013). Simple scaling of catastrophic landslide dynamics. *Science* 339 (6126), 1416–1419. doi:10.1126/science.1232887

Evans, S. G., and Delaney, K. B. (2011). Characterization of the 2000 Yigong Zangbo river (Tibet) landslide dam and impoundment by remote sensing, natural and artificial rockslide dams. *Geomorphology* 133, 543–559.

Fan, J. R., Zhang, X. Y., Su, F. H., Ge, Y. g., Tarolli, P., Yang, Z. y., et al. (2017). Geometrical feature analysis and disaster assessment of the Xinmo landslide based on remote sensing data. *J. Mt. Sci.* 14 (9), 1677–1688. doi:10.1007/s11629-017-4633-3

Gao, H. Y., Gao, Y., He, K., Li, B., Zhao, Z. N., Chen, L. C., et al. (2020). Impact and scraping effects of the high-elevation, long-runout "7.23" landslide in Shuicheng. Guizhou. *China Karst* 39 (4), 535–546. (in Chinese with English abstract). doi:10.11932/karst2020

Guo, C. B., Du, Y. B., Zhang, Y. S., Zhang, G. Z., Yao, X., Wang, K., et al. (2015). Geohazard effects of the Xianshuihe fault and characteristics of typical landslides in western sichuan. *Geol. Bull. China* 34 (1), 121–134. (in Chinese with English abstract). doi:10.3969/j.issn.1671-2552.2015.01.010

Guo, C. B., Montgomery, D. R., Zhang, Y. S., Zhong, N., Fan, C., Wu, R., et al. (2020). Evidence for repeated failure of the giant Yigong landslide on the edge of the Tibetan plateau. *Sci. Rep.* 10 (1), 14371. doi:10.1038/s41598-020-71335-w

Hao, Z. C., Ju, Q., Jiang, W. J., and Zhu, C. J. (2013). Characteristics and scenarios projection of climate change on the Tibetan plateau. *The Scientific World Journal.* 129793, 9, 2013. doi:10.1155/2013/129793

He, S. M., Bai, X. Q., Ouyang, C. J., and Wang, D. P. (2017). On the survey of giant landslide ai Xinmo village of Diexi town, Mao County, Sichuan Province, China. *J. Mt. Sci.* 35 (4), 598–603. (in Chinese with English abstract). doi:10.16089/j.cnki.1008-2786.000258

Hsu, K. J. (1975). Catastrophic debris streams (sturzstroms) generated by rockfalls. *Geol. Soc. Am. Bull.* 86 (1), 129–140. doi:10.1130/0016-7606(1975)86<129:cdssgb>2.0.co;2

Hu, G. T., Mao, Y. L., and Yang, J. H. (1992). On the accumulated strain energy close sliding piane and the elastic by impulsive motion along the initial path of bedrock's landslide. *J. Chang'an Univ. (Earth Sci. Ed.)* (4), 50–57.

Huang, R. Q., Chen, G. Q., and Tang, P. (2017). Precursor information of locking segment landslides based on transient characteristics. *Chin. J. Rock Mech. Eng.* 36 (3), 521–533. (in Chinese with English abstract).

Huang, R. Q. (2004). Mechanism of large scale landslides in western China. *Adv. Geoscience* 19 (3), 443–450. (in Chinese with English abstract). doi:10.3321/j.issn:1001-8166.2004.03.016

Hungr, O., Leroueil, S., and Picarelli, L. (2014). The Varnes classification of landslide types, an update. *Landslides* 11 (11), 167–194. doi:10.1007/s10346-013-0436-y

International Union of Geological Sciences Working Group on Landslides (1995). A suggested method for describing the rate of movement of a landslide. *Bull. Int. Assoc. Eng. Geol.* 52 (1), 75–78. doi:10.1007/bf02602683

Kojan, E., and Hutchinson, J. N. (1987). Mayunmarca rockslide and debris flow, Peru-ScienceDirect. *Dev. Geotechnical Eng.* 14, 315–353.

Li, C. L., and Kang, S. C. (2006). Review of studies in climate change over the Tibetan Plateau. *Acta Geogr. Sin.* 61 (3), 327–335. (in Chinese with English abstract). doi:10.3321/j.issn:0375-5444.2006.03.012

Li, F., Gao, Y. Q., Wan, X., Li, Q., Guo, D. L., Wang, P. L., et al. (2021). Earth's "three-Poles" climate change under global warming. *Trans. Atmos. Sci.* 44 (1), 1–11. (in Chinese with English abstract). doi:10.13878/j.cnki.dqkxxb.20201031003

Li, H., Shi, W. B., Zhu, Y. Q., and Peng, X. W. (2020). Study on the formation mechanism of "7.23" catastrophic landslide in Shuicheng County, Guizhou Province, China. *J. Nat. Disasters* 29 (6), 188–198. (in Chinese with English abstract). doi:10.13577/j.jnd.2020.0620

Li, J., Chen, N. S., Liu, M., Zhang, Y., Xiang, L., and Gao, Y. J. (2018). Analysis on main control factors of landslide-triggered debris flow in zhamunonggou, gully, on April 9th, 2000. *South North Water Transf. Water Conservancy Technol.* 16 (6), 187–193. (in Chinese with English abstract). doi:10.13476/j.cnki.nsbdqk.2018.0170

Li, J., Chen, N. S., Ouyang, C. J., Li, A. G., and Zuo, X. L. (2017). Volume of loose materials and analysis of possibility of blocking and dam break triggered by debris flows in Zhamunonggou. *J. Catastrophology* 32 (1), 80–84. (in Chinese with English abstract). doi:10.3969/j.issn.1000-811X.2017.01.014

Li, X., Li, S. D., Chen, J., and Liao, Q. L. (2008). Coupling effect mechanism of endogenic and exogenic geological processes of geological hazards evolution. *Chin. J. Rock Mech. Eng.* 27 (9), 1792. (in Chinese with English abstract). doi:10.3321/j.issn:1000-6915.2008.09.006

Lin, Q. W., Cheng, Q. G., Li, K., Wang, Y. F., and Liu, S. T. (2022). Review on fragmentation-related dynamics of rock avalanches. *J. Eng. Geol.*, 1–15. (in Chinese with English abstract). doi:10.13544/j.cnki.jeg.2021-0035

Liu, G. Q., and Lu, X. Y. (2000). Analysis of the giant landslide in Zhamunong gully, of Yigong river, Tibet. *Tibet Sci. Technol.* 7 (4), 15–17. (in Chinese with English abstract).

Liu, G. Q., Lu, X. Y., and Li, Y. (2001). Analysis of landslide and debris flow in Zhamunong gully. *Northeast water Resour. hydropower* 19 (6), 49–50. (in Chinese with English abstract). doi:10.1007/s11069-017-3073-2

Liu, N. (2000). Scientifically formulate the disaster reduction plan for Yigong landslide blocking the river in Tibet. *China Water Resour.* 51 (7), 37–38. (in Chinese with English abstract).

Liu, W., and He, S. M. (2018). Dynamic simulation of a mountain disaster chain: Landslides, barrier lakes, and outburst floods. *Nat. Hazards (Dordr)* 90 (5), 757–775. doi:10.1007/s11069-017-3073-2

Liu, W., Wang, Y. T., Tian, D. S., Yin, Z. C., and Kwang, J. (2002). Detection of white spot syndrome virus (WSSV) of shrimp by means of monoclonal antibodies (MAbs) specific to an envelope protein (28 kDa). *Dis. Aquat. Organ.* 13 (3), 11–18. (in Chinese with English abstract). doi:10.3354/dao049011

Liu, Z., Li, B., He, K., Gao, Y., and Wang, W. P. (2020). Analysis of dynamic response characteristics of Yigong landslide in Tibet under earthquake. *J. Geomechanics* 26 (4), 471–480. (in Chinese with English abstract). doi:10.12090/j.issn.1006-6616.2020.26.04.040

Lu, X. Y., Yang, M. G., Zhao, D., and Cai, G. Z. (2000). Analysis of the causes and collapse of a very large landslide in zhamunonggou of Yigong zangbu in Tibet. *Proc. Sixth Natl. Eng. Geol. Conf.*, 263–264. (in Chinese with English abstract).

Lv, J. L., Wang, Z. H., and Zhou, C. H. (2003a). Discussion on the occurrence of Yigong landslide in Tibet. *Earth Sci.* 47 (1), 107–110. (in Chinese with English abstract). doi:10.3321/j.issn:1000-2383.2003.01.018

Lv, J. T., Wang, Z. H., and Zhou, C. H. (2003b). A tentative discussion on the monitoring of the Yigong landslide-blocked lake with satellite remote sensing technique. *Acta Geosci. Sin.* 24 (4), 363–368. (in Chinese with English abstract). doi:10.3321/j.issn:1006-3021.2002.04.014

Mcguire, B. (2010). Potential for a hazardous geospheric response to projected future climate changes. *Phil. Trans. R. Soc. A* 368, 2317–2345. doi:10.1098/rsta.2010.0080

Ouyang, C. J., An, H. C., Zhou, S., Wang, Z., Su, P., Wang, D., et al. (2019). Insights from the failure and dynamic characteristics of two sequential landslides at baige village along the jinsha river, China. *Landslides* 16, 1397–1414. doi:10.1007/s10346-019-01177-9

Ouyang, C. J., Zhou, K., Xu, Q., Yin, J., Peng, D., Wang, D., et al. (2017). Dynamic analysis and numerical modeling of the 2015 catastrophic landslide of the construction waste landfill at Guangming, Shenzhen, China. *Landslides* 14, 705–718. doi:10.1007/s10346-016-0764-9

Quan, X. R., Huang, Y. H., and Liu, C. (2021). Numerical simulation study on seismic magnification effect of V-shaped deep-cut valley on sichuan-tibet railway line. *Geoscience* 35 (1), 38–46. (in Chinese with English abstract). doi:10.19657/j.geoscience.1000-8527.2021.020

Ren, J. W., Shan, X. J., Shen, J., Ge, S., Zha, S., Deng, G. Y., et al. (2001). Geological characteristics and kinematics of rock fall- landslide in Yigong, Southeastern Tibet. *Geol. Rev.* 66 (6), 642–647. (in Chinese with English abstract). doi:10.3321/j.issn.0371-5736.2001.06.013

Shang, Y. J., Yang, Z. F., Li, L. H., Liu, D., Liao, Q., and Wang, Y. (2003). A super-large landslide in Tibet in 2000: Background, occurrence, disaster, and origin. *Geomorphology* 54, 225–243. doi:10.1016/s0169-555x(02)00358-6

Shao, C. R. (2009). *Seismicity of the yarlung tsangpo grand canyon region*. ChinaChina Earthquake Administration: Institute of Geophysics. (in Chinese with English abstract).

Stead, D., and Eberhardt, E. (2013). Understanding the mechanics of large landslides. *Ital. J. Eng. Geol. Environ. Book Ser.* (6), 85–112.

Tang, F. T., Song, J., Cao, Z. Q., Deng, Z. H., Wang, M., Xiao, G. R., et al. (2010). The movement characters of main faults around eastern himalayan syntaxis revealed by the latest GPS data. *Chin. J. Geophys.* 53 (9), 2119–2128. (in Chinese with English abstract). doi:10.3969/j.issn.0001-5733.2010.09.012

Turzewski, M. D., Huntington, K. W., and Leveque, R. J. (2019). The geomorphic impact of outburst floods: Integrating observations and numerical simulations of the 2000 Yigong flood, eastern Himalaya. *J. Geophys. Res. Earth Surf.* 124 (5), 1056–1079. doi:10.1029/2018jf004778

Wan, H. B. (2000). Overview of the rescue and mitigation of the giant landslide in Yigong, Tibet. *China J. Disaster Reduct.* 10 (4), 28–31. (in Chinese with English abstract). doi:10.3321/j.issn:1001-6791.2000.03.016

Wang, S. J. (2002). Coupling of earth's endogenic and exogenic geological processes and origins on serious geological disasters. *J. Eng. Geol.* 10 (2), 115–117. (in Chinese with English abstract). doi:10.3969/j.issn.1004-9665

Wang, Z. H. (2008). A thunder at the beginning of the 21st century-the giant Yigong landslide in *The tenth international symposium on landslides and engineered slopes*, 1068–1075.

Wang, Z. H., and Lv, J. T. (2002). Satellite monitoring of the Yigong landslide in Tibet, China. *Proc. SPIE – Int. Soc. Opt. Eng.* 4814, 34–38.

Wang, Z. H., and Lv, X. J. (2001). Understand Yigong landslide in Tibet based on the satellite image. *Natl. Remote Sens. Bull.* 5 (4), 312–316. (in Chinese with English abstract).

Wang, Z. H. (2005). Remote sensing for landslide in China. *Remote Sens. Nat. Resour.* 18 (1), 1–7. (in Chinese with English abstract). doi:10.3969/j.issn.1001-070X.2005.01.001

Wang, Z. H. (2006). Large scale individual landslide remote sensing. *Geosci. Front.* 13 (5), 516–523. (in Chinese with English abstract). doi:10.3321/j.issn.1005-2321.2006.05.018

Wang, Z. L., Zhao, X. F., Guo, X. D., and Huang, Y. Z. (1996). Response of permafrost to climate change on the Tibetan plateau. *J. Glaciol. Geocryol.* 18 (S1), 157–165. (in Chinese with English abstract).

Wang, Z., Zhao, Y. C., Liu, X. J., and Li, B. (2021). Evolution analysis and deformation monitoring of yigong landslide in Tibet with optical remote sensing and InSAR. *Geomat. Inf. Sci. Wuhan Univ.* 46 (10), 1569–1578. (in Chinese with English abstract). doi:10.13203/j.whugis20210168

Wen, B. P., Wang, S. J., Wang, E. Z., and Zhang, J. (2004). Characteristics of rapid giant landslides in China. *Landslides* 1 (4), 247–261. doi:10.1007/s10346-004-0022-4

Wu, W. Y., and Xu, C. (2018). A new inventory of landslide triggered by the 2014 ludian M$_W$6.2 earthquake. *Seismol. Geol.* 40 (5), 1140–1148. (in Chinese with English abstract). doi:10.3969/j.issn.0253-4967.2018.05.013

Xia, S. W. (2018). *Study on three dimensional numerical simulation of Yigong rock avalanche and it's dam breach*. Shanghai: Shanghai Jiaotong University. (in Chinese with English abstract).

Xu, Q., Wang, S. T., Chai, H. J., Zhang, Z. Y., and Dong, S. M. (2007). *The rock avalanche-flow landslide event in Yigong of Tibet*. The first academic conference on rock mechanics and engineering examples in China. Sanya: Chinese Society of Rock Mechanics and Engineering, 41–46. (in Chinese with English abstract). doi:10.13203/j.whugis20190088

Xu, Q., Dong, X. J., and Li, W. L. (2019). Integrated space-air-ground early detection, monitoring and warning system for potential catastrophic geohazards. *Geomatics Inf. Sci. Wuhan Univ.* 44 (7), 957–966. (in Chinese with English abstract). doi:10.13203/j.whugis20190088

Xu, Q., Li, W. L., Dong, X. J., Xiao, X. X., Fan, X. M., and Pei, X. J. (2017). The Xinmocun landslide on June 24, 2017 in Maoxian, Sichuan: Characteristics and failure mechanism. *J. Rock Mech. Eng.* 36 (11), 2612–2628. (in Chinese with English abstract). doi:10.13722/j.cnki.jrme.2017.0855

Xu, Q., Shang, Y. J., Asch, T. V., Wang, S., Zhang, Z., and Dong, X. (2012). Observations from the large, rapid Yigong rock slide – debris avalanche, southeast Tibet. *Can. Geotech. J.* 49 (5), 589–606. doi:10.1139/t2012-021

Xu, Q. (2020). Under standing the landslide monitoring and early warning: Consideration to practical issue. *J. Eng. Geol.* 28 (2), 360–374. (in Chinese with English abstract). doi:10.13544/j.cnki.jeg.2020-025

Xu, X. W., Han, Z. J., Yang, X. P., Zhang, S. M., Yu, G. H., Zhou, B. G., et al. (2016). *Seismic tectonic map of China and adjacent areas*. Beijing: Seismological PressDb. doi:10.12031/activefault.China.250.2016

Xue, G. F., Liu, N., Jiang, N. M., and Yang, Q. Z. (2000). *Investigation on the giant landslide dam on the Yigong river of Tibet and studies on mitigation of the catastrophe caused by the dam failure*. Wuhan: The Sixth National Conference on Rock Mechanics and Engineering, 640–644. (in Chinese with English abstract).

Yao, T. D., Liu, X. D., and Wang, N. L. (2000). The magnitude of climate change in the Tibetan plateau region. *Chines Sci. Bull.* 51 (1), 98–106. (in Chinese with English abstract). doi:10.3321/j.issn:0023-074X.2000

Yao, T. D., Yang, Z. H., and Liu, J. S. (1994). Temperature rise of qinghai Tibet plateau revealed by ice core records. *Sci. Bull.* 45 (5), 438–441. (in Chinese with English abstract).

Yin, Y. P., (2000). Study on characteristics and disaster reduction of giant landslide of Bomi Yigong expressway in Tibet. *Hydrogeology Eng. Geol.* 44 (4), 8–11. (in Chinese with English abstract). doi:10.3969/j.issn.1000-3665.2000.04.003

Yin, Y. P. (2008). Researches on the geo -hazards triggered by wenchuan earthquake, sichuan. *J. Eng. Geol.* 16 (4), 433–444. (in Chinese with English abstract). doi:10.3969/j.issn1004-9665.2008.04.001

Yin, Y. P., and Wang, W. P. (2020). A dynamic erosion plowing model of long run-out landslides initialized at high locations. *Chin. J. Rock Mech. Eng.* 08–151309. (in Chinese with English abstract). doi:10.13722/j.cnki.jrme.2020.0062

Yin, Y. P., Wang, W. P., Zhang, N., Yan, J. K., Wei, Y. J., and Yang, L. W. (2017). Long runout geological disaster initiated by the ridge-top rockslide in a strong earthquake area: A case study of the Xinmo landslide in Maoxian County, Sichuan Province. *Geol. China* 44 (5), 827–841. (in Chinese with English abstract). doi:10.12029/gc20170501

Yin, Y. P., and Xing, A. G. (2012). Aerodynamic modeling of the Yigong gigantic rock slide-debris avalanche, Tibet, China. *Bull. Eng. Geol. Environ.* 71 (1), 149–160. doi:10.1007/s10064-011-0348-9

Zhang, M., and Yin, Y. P. (2013). Dynamics, mobility-controlling factors and transport mechanisms of rapid long-runout rock avalanches in China. *Eng. Geol.* 167 (12), 37–58. doi:10.1016/j.enggeo.2013.10.010

Zhang, M., Yin, Y. P., Wu, S. R., and Zhang, Y. S. (2010). Development status and prospect of kinematics of long runout rock avalaches. *J. Eng. Geol.* 18 (6), 805–817. (in Chinese with English abstract). doi:10.3969/j.issn.1004-9665.2010.06.001

Zhang, Y. S., Guo, C. B., Yao, X., Yang, Z. H., Wu, R. A., and Du, G. L. (2016). Research on the geohazard effect of active fault on the eastern margin of the Tibetan Plateau. *Acta Geosci. Sin.* 37 (03), 277–286. (in Chinese with English abstract). doi:10.3975/cagsb.2016.03.03

Zhang, Y. S., Ren, S. S., Bi, J. B., Li, J., Gao, Y., Wu, R., et al. (2022). Multi-period formation and possible high-position hazards of Chada gully deposits on the eastern margin of Tibetan Plateau. *Eng. Geol.* 305, 106712. doi:10.1016/j.enggeo.2022.106712

Zheng, G., Xu, Q., Liu, X. W., Li, Y. C., Dong, X. J., Ju, N. P., et al. (2020). The Jichang landslide on July 23, 2019 in Shuicheng, Guizhou: characteristics and failure mechanism. *J. Eng. Geol.* 28 (3), 541–556. (in Chinese with English abstract). doi:10.13544/j.cnki.jeg.2020-083

Zhou, C. H., Yue, Z. Q., Lee, C. F., Zhu, B. Q., and Wang, Z. H. (2001). Satellite image analysis of a huge landslide at yi gong, Tibet, China. *Q. J. Eng. Geol. Hydrogeo.* 34 (4), 325–332. doi:10.1144/qjegh.34.4.325

Zhou, G. G. D., Roque, P. J. C., Xie, Y. X., Song, D., Zou, Q., and Chen, H. (2020). Numerical study on the evolution process of a geohazards chain resulting from the Yigong landslide. *Landslides* 17 (17), 2563–2576. doi:10.1007/s10346-020-01448-w

Zhou, G. Y., Li, Y. Z., and Li, P. (2000). ADCP monitoring in emergency treatment of Yigong massive landslide in Tibet. *People's Yangtze River* 31 (9), 30–32. (in Chinese with English abstract). doi:10.16232/j.cnki.1001-4179.2000.09.012

Zhou, J. W., Cui, P., and Hao, M. H. (2016). Comprehensive analyses of the initiation and entrainment processes of the 2000 Yigong catastrophic landslide in Tibet, China. *Landslides* 13 (1), 39–54. doi:10.1007/s10346-014-0553-2

Zhou, X., Xing, A. G., and Chen, L. J. (2010). Numerical analysis on the flying Yigong high-speed and long runout landslide at short-range stage. *J. Shanghai Jiaot. Univ.* 44 (6), 833–838. (in Chinese with English abstract). doi:10.16183/j.cnki.jsjtu.2010.06.024

Zhou, Z. Q., and Li, H. G. (2000). Giant landslide and disaster prevention and mitigation measures in Yigong, Tibet. *Water Resour. Hydropower Eng.* 42 (12), 47–50. (in Chinese with English abstract). doi:10.3969/j.issn.0559-9342.2000.09.016

Zhu, B. Q., and Nie, Y. P. (2001). Using satellite remotely sensed data to monitor Yigong tremendous high-speed landslide. *J. Nat. Disasters* 10 (3), 103–107. (in Chinese with English abstract). doi:10.3969/j.issn.1004-4574.2001

Zhu, C. M., and Zhang, C. X. (2015). Preliminary discussion on treatment of geological hazard in Zhamunong valley in Tibet. *Yangtze River* 46 (18), 26–28. (in Chinese with English abstract). doi:10.16232/j.cnki.1001-4179. 2015.18.007

Zhu, P. Y., Wang, C. H., and Tang, B. G. (2000). The deposition characteristic of supper debris flow in Tibet. *J. Mt. Sci.* 18 (5), 453–456. (in Chinese with English abstract). doi:10.3969/j.issn.1008-2786.2000.05.009

Zhuang, Y., Xang, A. G., Leng, Y. Y., Bilal, M., Zhang, Y., Jin, K., et al. (2021). Investigation of characteristics of long runout landslides based on the multi-source data collaboration: A case study of the Shuicheng basalt landslide in guizhou, China. *Rock Mech. Rock Eng.* 54, 3783–3798. doi:10.1007/s00603-021-02493-0

Zhuang, Y., Yin, Y. P., Xing, A. G., and Jin, K. (2020). Combined numerical investigation of the Yigong rock slide-debris avalanche and subsequent dam-break flood propagation in Tibet, China. *Landslides* 17 (9), 2217–2229. doi:10.1007/s10346-020-01449-9